Available online at www.sciencedirect.com
SCIENCE DIRECT®
Pergamon
Acta Materialia 51 (2003) 5743–5774
Acta MATERIALIA
www.actamat-journals.com

Mechanical behavior of nanocrystalline metals and alloys☆

K.S. Kumar [a,*], H. Van Swygenhoven [b], S. Suresh [c]

[a] *Division of Engineering, Brown University, Providence, RI 02912, USA*
[b] *Paul Scherrer Institute, Villigen-PSI, CH-5232, Switzerland*
[c] *Department of Materials Science and Engineering, Massachusetts Institute of Technology, Cambridge, MA 02139, USA*

Accepted 31 August 2003

Abstract

Nanocrystalline metals and alloys, with average and range of grain sizes typically smaller than 100 nm, have been the subject of considerable research in recent years. Such interest has been spurred by progress in the processing of materials and by advances in computational materials science. It has also been kindled by the recognition that these materials possess some appealing mechanical properties, such as high strength, increased resistance to tribological and environmentally-assisted damage, increasing strength and/or ductility with increasing strain rate, and potential for enhanced superplastic deformation at lower temperatures and faster strain rates. From a scientific standpoint, advances in nanomechanical probes capable of measuring forces and displacements at resolutions of fractions of a picoNewton and nanometer, respectively, and developments in structural characterization have provided unprecedented opportunities to probe the mechanisms underlying mechanical response. In this paper, we present an overview of the mechanical properties of nanocrystalline metals and alloys with the objective of assessing recent advances in the experimental and computational studies of deformation, damage evolution, fracture and fatigue, and highlighting opportunities for further research.

Keywords: Nanocrystalline materials; Mechanical properties; Grain boundaries; Grain refining; Modeling

1. Introduction

The processing, structure and properties of metallic materials with grain size in the tens to several hundreds of nanometer range are research areas in which there has been a considerable increase in interest over the past few years. The application of grain refinement as a powerful tool to design microstructures with superior properties and performance has long been the focus of metallurgical research; numerous papers with this theme have been published in Acta Metallurgica/Materialia over the past fifty years. However, several major drivers have contributed to the rapid increase in research into nanocrystalline metals and alloys in recent years. Advances in the processing of alloys

* Corresponding author. Tel.: +1-401-863-2862; fax: +1-401-863-7677.
E-mail address: sharvan_kumar@brown.edu (K.S. Kumar).
☆ The Golden Jubilee Issue—Selected topics in Materials Science and Engineering: Past, Present and Future, edited by S. Suresh

1359-6454/$30.00
doi:10.1016/j.actamat.2003.08.032

along with the precipitous rise in the sophistication of routine, commonly available tools capable of characterizing materials with force, displacement and spatial resolutions as small as picoNewton (pN = 10^{-12} N), nanometer (nm = 10^{-9} m) and Angstrom (0.1 nm), respectively, have provided unprecedented opportunities to probe the structure and mechanical response of alloys in the nanoscale regime. In addition, major improvements in computer hardware and software have facilitated simulations of the structure and deformation of materials with a degree of sophistication and refinement unimaginable as recently as a decade ago. These factors, along with major national initiatives in the broad area of nanotechnology in the United States, Europe and Japan, have further accelerated interest in the study of nanocrystalline metals and alloys for a wide variety of structural and functional applications. In the Millennium Special Issue of Acta Materialia, published in 2000, Gleiter [1] presented a comprehensive overview of nanostructured materials, with a specific emphasis on the connections between structure and functional properties. A critical appraisal of the current state of understanding and of possible avenues for further exploration in the broad field of mechanical properties of nanoscrystalline metals and alloys, particularly in the context of processing-structure-property connections, seems appropriate at this time.

For the purpose of discussion throughout this paper, we define nanocrystalline (nc) metals and alloys as those with an average grain size and range of grain sizes smaller than 100 nm. Ultrafine crystalline (ufc) metals and alloys are taken to be those with an average grain size in the 100–1000 nm range, whereas their microcrystalline (mc) counterparts have average grain dimension of a micrometer or larger. It is important to note in this context that the mechanisms of deformation and the properties of the nc material not only depend on the average grain size, but are also strongly influenced by the grain size distribution and the grain boundary structure (e.g., low-angle versus high-angle grain boundaries).

Some appealing characteristics of nc metals and alloys with potential significance for engineering applications include ultra-high yield and fracture strengths, decreased elongation and toughness, superior wear resistance, and the promise of enhanced superplastic formability at lower temperatures and faster strain rates compared to their mc counterparts. Consider, for example, the variation of flow stress as a function of grain size from the mc to the nc regime, which is schematically shown in Fig. 1. In many mc and ufc metals and alloys with average grain size of 100 nm or larger, strengthening with grain refinement has traditionally been rationalized on the basis of the so-called Hall-Petch mechanism [2–4]. Here pile-up of dislocations at grain boundaries is envisioned as a key mechanistic process underlying an enhanced resistance to plastic flow from grain refinement. As the microstructure is refined from the mc and ufc regime into the nc regime, this process invariably breaks down and the flow stress versus grain size relationship departs markedly from that seen at higher grain sizes. With further grain refinement, the yield stress peaks in many cases at an average grain size value on the order of 10 nm or so. Further decrease in grain size can cause weakening of the metal. Although there is a growing body of experimental evidence pointing to such unusual deformation responses in nc materials, the underlying mechanisms are not well understood. Consequently, there is a concerted global effort underway using a combination of novel processing routes, experiments and large-scale computations to

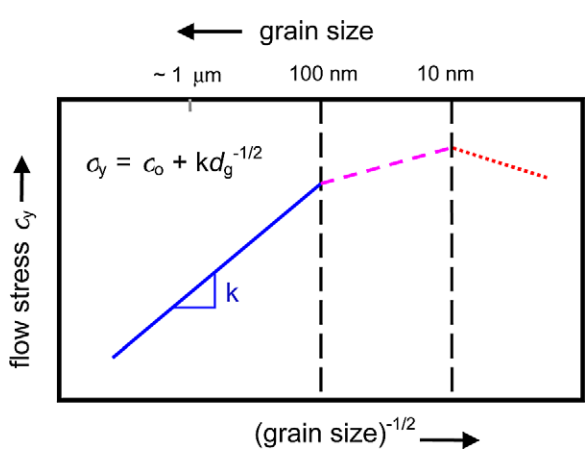

Fig. 1. Schematic representation of the variation of yield stress as a function of grain size in mc, ufc and nc metals and alloys.

develop deeper insights into the various aspects of these phenomena.

In this overview, we focus attention on the mechanical behavior of nc metals and alloys. The majority of available experimental and computational results on this topic pertain to face-centered cubic (fcc) structure, and hence the results highlighted primarily deal with this class of metals; however, references to other crystal structures are included, wherever available. The paper is broadly divided into five major sections: (1) processing, (2) grain boundary structure, (3) mechanical properties, (4) deformation mechanisms, and (5) fracture mechanisms. An attempt is made to compare the behavior of nc metals with those of ufc and mc metals, and to assess computational predictions in light of experimental observations, wherever possible. It is worth noting that the topic of grain refinement also constitutes an important aspect of the broad area of superplasticity in metals and alloys. However, available results in this area primarily deal with ufc materials and consequently, it is not taken up for discussion in this overview. Examples of recent activity in the area of superplasticity of ufc materials can be found in [5–11].

2. Processing of nanocrystalline metals and alloys

Several laboratory-scale processing techniques are currently available to produce nc and ufc materials. They can be generally classified into the following four groups: mechanical alloying (including cryomilling) and compaction [12–15], severe plastic deformation [16], gas-phase condensation of particulates and consolidation [17–19], and electrodeposition [20–22]. Whereas the first two methods typically tend to yield material with ultra-fine grain sizes, the latter two techniques are capable of producing material with mean grain sizes in the tens of nm. A fifth technique which can, in principle, facilitate the production of a nc alloy entails controlled crystallization of a material capable of forming an initially fully amorphous metallic glass, particularly if the metallic glass can be produced in bulk form. This approach is attractive for producing controlled two-phase microstructures [23,24], but due to the nature of the process, the technique is limited to glass-forming compositions. With this approach, nanocrystallites can be formed either by controlled thermal annealing (e.g. in [25–27] and/or by severe mechanical deformation at the bulk [28] or local [29] level.

Mechanical alloying, and specifically cryomilling in a liquid nitrogen medium, has been used to produce ultra-fine-grained materials in reasonable quantities and the resulting powder has been warm/hot consolidated to full/nearly-full density with insignificant grain growth. The method has been particularly successful with aluminum alloys [14,15] and the presence of fine oxides/nitrides that result from the milling process is key to maintaining the fine grain size during consolidation. While the advantage of the process lies in its ability to produce reasonable size billets of material, its principal disadvantages include the inability to control material purity and obtaining full density. Some of the shortcomings associated with material purity can be offset by using the approach of severe deformation of bulk material (as, for example, via torsion, multiple extrusion or multiple forging) where material purity is limited only by that of the starting material, but the typical grain sizes obtained still remain in the 150–300 nm regime or more. Metals and alloys have been successfully processed by this route and include Al alloy 01420, Cu, Ni and Ti and its alloys (such as Ti-6Al-4V), steels and intermetallic compounds. Due to extensive and repeated deformation processing, the grain boundaries are highly dislocated. The microstructure is usually characterized by larger grains (having high-angle grain boundaries) with an internal sub-grain boundary structure. A comprehensive review by Valiev et al. [16] discusses the various metallurgical aspects of materials produced by severe plastic deformation.

Gas-phase condensation or inert gas condensation [17–19] has been used in a limited way to produce nc metals such as Cu, Ni and Pd. Here, powder particles with grain size in the 5–50 nm regime are produced by condensing from the vapor phase, and the particles are then consolidated in a die using high pressures and, in some cases, with additional thermal energy. The process has several limitations including specimen volume and yield,

purity issues particularly in the vicinity of the particle boundaries, incomplete densification/porosity (resulting in specimens with densities lower then 99% of the theoretical density), and difficulties associated with retaining the fine grain size during consolidation. Improvements to the process have been reported [18], but considerable further advances in process optimization are needed before this method can find commercialization. The process, however, is capable of providing a microstructure that is usually texture-free and consisting of equiaxed grains. Recently it has been shown that the density of the specimens can be increased by cold rolling, while retaining the equiaxed, texture-free microstructure without a change in grain size [30].

Electrodeposition (direct current and pulsed) has been used to produce sheets of nc metals (such as Ni, Co, Cu) and binary alloys (such as Ni-Fe; Ni-W) [20–22,31–34]. Grain size can be controlled and sheets with thickness of 100 μm or more and grain size of 20–40 nm are routinely produced [34]. A bright field image (Fig. 2(a)) shows the typical microstructure of electrodeposited nc Ni with an average grain size of about 30–40 nm. Alloying with W has enabled further reductions in grain size down to 10 nm or less [33], and a representative bright field micrograph of the structure of a Ni-W alloy is shown in Fig. 2(b). Grain size distribution in these materials often tends to be narrow with the maximum grain size not exceeding 80 nm for a material with a mean grain size of 20–30 nm [35]. The use of saccharin in the plating bath to produce nc grains often results in carbon and sulfur as impurities in the material [36,37]; furthermore, hydrogen levels in the deposits can be substantial and it is not uncommon to find hydrogen-filled nano-bubbles in the microstructure even though full-density is measured within the errors of the Archimedes technique. Process control dictates the presence or absence of a columnar structure, and the presence of clusters of grains with minimal misorientation between each other has been reported [35]. Likewise, process parameters influence the texture of the deposit, and in the case of Ni produced by pulsed electrodeposition, El-Sherik and Erb [37] report a change in texture with decreasing grain size, an observation also made by

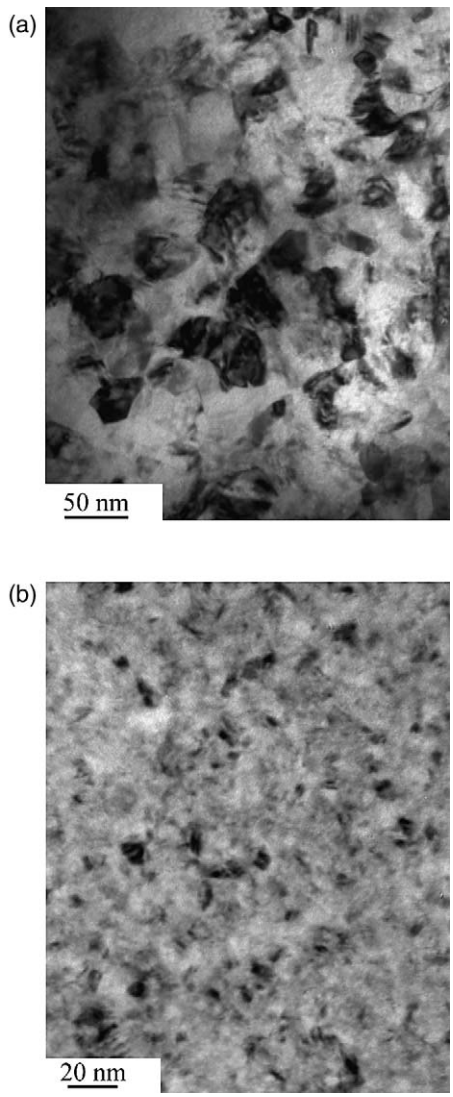

Fig. 2. Bright field TEM images of electrodeposited (a) nc-Ni with an average grain size around 30 nm, and b) nc-Ni-W with an average grain size of ~10 nm.

Ebrahimi and coworkers [36]. Electrodeposition has also successfully been used to produce nc metallic coatings on complex shapes [34].

In recent years, more effort has been devoted to improving the synthesis of nc-metals by electrodeposition rather than by inert gas condensation/compaction, primarily because of the problems associated with attaining full density via the latter approach. Reports on the mechanical

properties and deformation response of nc metals and alloys in earlier papers were often influenced, in many cases, by the presence of porosity (samples densities were frequently lower then 98%) and impurities. Furthermore, even at present, the microstructure of a metal produced by a particular technique appears to vary from batch to batch and frequently, microstructures have not been characterized to the level necessary for rigorous interpretation of the observed results. For example, very small pores of tens of nm size scale, commonly referred to as nanovoids, are often present in the material, and they can have a significant influence on the measured mechanical properties. These nanovoids are below the detection limits of density measurements and can only be inferred by positron annihilation [38,39]. Not accounting properly for the possible direct effects of such processing-induced defects on the mechanical response has led to numerous contradictory results in the published literature (examples of which are discussed in [40,41]). These factors have made it difficult to identify, in many cases, the intrinsic deformation characteristics of materials with grain sizes in the nanometer size scale and therefore, to obtain a clear mechanistic understanding of their mechanical response.

3. Grain Boundaries (GB) in nanocrystalline metals and alloys

Relative to mc metals and alloys (i.e. materials with grain size in the micrometer range), nc materials contain a higher fraction of grain boundary volume (for example, for a grain size of 10 nm, between 14 and 27% of all atoms reside in a region within 0.5–1.0 nm of a grain boundary); therefore, grain boundaries are thought to play a significant role in the deformation of these materials. These boundaries act as sources and sinks for dislocations and facilitate such stress-relief mechanisms as grain boundary sliding. Given this trend, there are surprisingly few experimental studies that have sought to examine the structure of grain boundaries in nc metals and alloys. Earlier postulates that there exists an amorphous layer (or variously called an "extended disordered region" or "randomly arranged atoms") at grain boundaries of nc metals and alloys [17,42–46] have been questioned based on experimental observations [41,47,48] and computations (a more detailed discussion follows below and also in [49]). High-resolution images of grain boundaries in electrodeposited Ni with an average grain size of 30–40 nm (Fig. 3(a),(b)) and in vapor-phase condensed and consolidated nc Cu (Fig. 3(c),(d)) confirm that crystallinity is maintained right up to the boundary. Gleiter [17] points to the need for caution in correlating grain boundary structures observed by high resolution TEM to structures in bulk nc materials due to possible influence of relaxation; this has, however, been shown not to be an issue by Siegel and Thomas [47] and by the calculations of Mills and Daw [50]. For Ni-W nanocrystalline alloys, Schuh et al. [33] report the existence of a finite non-crystalline region at grain boundaries that were examined by high-resolution microscopy but enough evidence was not presented there for its prevalence at all boundaries. Moreover, it is not clear whether this is a chemical effect arising from the W in the alloy or if it is a direct consequence of the extremely fine grain size (typically < 10 nm). Chemical segregation of impurities or alloying additions to grain boundaries and its effects on structure (or lack thereof), deformation and fracture have not been examined. It is also not known if such effects provide a preferred crack path at the very high strength levels typical of such fine-grained materials. Grain boundaries in the as-deposited material (in the case of electrodeposition), and in as-deformed material (in the case of ufc alloys produced by severe plastic deformation) can be in a non-equilibrium state and in the latter case, can also have a high density of dislocations. Such structures are difficult to characterize in the transmission electron microscope and their metastable nature and spatial non-uniformity often make clear interpretation of observations difficult. Simulations [51] of the deformation response of nc-Ni containing grain boundaries with various levels of disorder (i.e. equilibrium versus non-equilibrium) that mimic the as-deposited and annealed conditions, have shown that grain boundary relaxation by a process such as annealing leads to a decrease in plasticity and increase in strength. While the experimental results

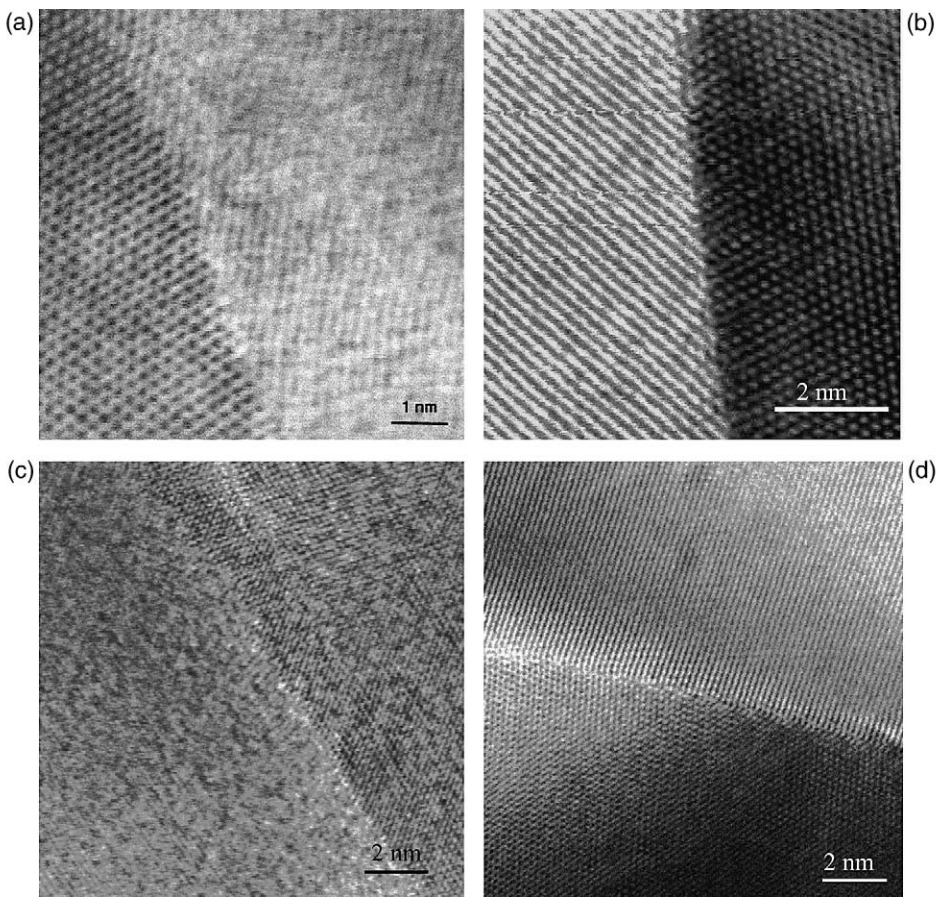

Fig. 3. High resolution TEM images of grain boundaries in (a,b) electrodeposited nc-Ni, and (c,d) nc-Cu produced by gas-phase condensation. In all cases, crystallinity is maintained right up to the boundary and no second phase is observed.

on inert gas condensed nc-Cu [52] support the simulation results, the results of Ebrahimi et al. [22] on electrodeposited Cu (grain size 175–250 nm) suggest otherwise. It is possible that at these larger grain sizes (as opposed to at 10–20 nm grain size), the structure of the grain boundary is already close to equilibrium. Further experimental data are needed to verify the suggestions from computer simulations [51].

The use of large-scale molecular dynamics (MD) to obtain atomic level structural information on the grain boundaries in nc fcc metals [46,49] has significantly enhanced the understanding realized from experiments. Most simulations have been performed on fcc pure metals with dislocation-free grains; Keblinski et al. [53] have also studied nc Si. A fully three-dimensional (3D) nc grain boundary (GB) network may be constructed in one of several ways: simulations of material synthesis can be accomplished (a) by cluster assembly followed by compaction [54,55], (b) by cooling from the melt with pre-defined crystallization seeds [46,56], or (c) by using space filling techniques based on Voronoi construction [57] with randomly generated seeds and orientations in order to prepare samples with mainly high angle grain boundaries [49,58,59] or with restrictions on crystallographic orientations in order to obtain tex-

tured samples [60]. The maximum grain size that has been simulated in full 3D GB networks is 30nm [58] for a sample containing 15 grains. All simulations apply periodic boundary conditions, a replica technique that mimics bulk conditions. In order to increase the grain size in simulations, samples with a two-dimensional (2D) columnar GB network containing four hexagonal-shaped fcc columnar-grains textured around the [1$\bar{1}$0] axis have been constructed in which the periodic boundary conditions are applied on ten atomic planes in the columnar direction. In these samples the GBs are perpendicular to the tensile direction and contain only twist-free misorientations [61,62] and therefore cannot mimic a general nc GB network. The GBs made by cooling from the melt using pre-existing fcc crystal seeds would be expected to have a different non-equilibrium state relative to those derived from a space-filling technique. Furthermore, even within one technique, the final GB structure will depend on the relaxation time and temperature, as has been shown for Voronoi constructed samples [51].

Simulations show that different patterns and degrees of order with different length scales are obtained when different criteria are used for GB atoms [63]. This is demonstrated in Fig. 4a-d. The three upper images (Fig. 4(a)–(c)) show a section of the GB viewed perpendicular to the GB plane, whereas Fig. 4(d) shows a section viewed along the GB plane where a general GB with an irreducible 50° misorientation around a (110) axis of the lower grain is shown. In Fig. 4(a), the GB is defined by those atoms, which according to the medium range order (MRO) analysis [49,64] do not have the fcc structure. In Fig. 4(b), the GB is defined by those atoms that are positional disordered (PD) i.e. atoms which cannot be assigned to a particular lattice site of the neighboring fcc grains [65]. In Fig. 4(c), the GB is defined by the atoms having an excess energy higher than the latent heat of melting. The view along the GB plane in Fig. 4(d) shows the coherence among (111) crystallographic planes of the lower grain and (100) crystallographic planes of the upper grain, with a regular pattern of misfit areas. From Fig. 4, it is clear that claiming the existence of amorphous GBs on the basis of a single criterion, such as excess energy [46,53], is not justified. Using the above-mentioned criteria, it has been demonstrated that pure metallic samples resulting from a Voronoi construction have grain boundaries that are fundamentally the same as their coarse-grained counterparts [49]. For all types of misfit, a large degree of structural coherence is observed and misfit accommodation occurs in somewhat regular patterns, with the misfit areas containing a larger degree of disorder.

Further important information on grain boundaries in nc materials can be obtained by the direct calculation of the variation of the internal stress [66,67] and the free volume in GBs [68]. The local pressure variations, made up of adjacent regions of high compression and dilatation (the colour code ranges from red for 2 GPa to blue for –2 GPa), are shown in Fig. 5(a) for the GB discussed in Fig. 4 (Fig. 5(b) shows the stress distribution after 0.5 nsec of tensile deformation—the details pertaining to Fig. 5(b) are presented in the Deformation Mechanism section). The stress concentrations observed in such a GB would be expected to produce inhomogeneous strain inside the grains, a parameter that is experimentally obtained from peak broadening in X-ray diffraction. The amount of free volume and its distribution also influence atomic mobility in GBs. It is also possible to calculate positron life times in simulated samples which can then be compared to experimental data [39,68]. Such calculations for samples synthesized in the computer by a space-filling technique [68] show that they have densities similar to the experimental values (99.26% for a 20 nm sample), but contain no nano-scale voids. Instead, they contain small amounts of free volume of sizes in-between that for a single vacancy and of the perfect crystal. However, in nearly all experimental samples, nano-scale voids containing 5 to 20 vacancies have been identified in positron lifetime measurements–even when the samples are fully dense as determined by the Archimedes principle [38,39,68]. This important difference in free volume distribution between simulated and experimental samples should be addressed in order to render the computational models more representative of experiments.

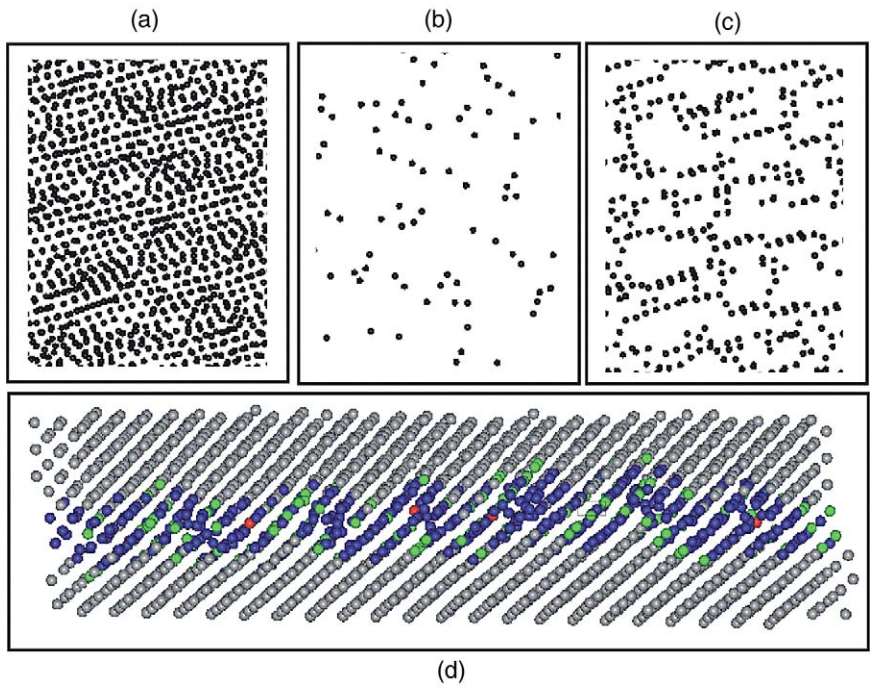

Fig. 4. Perpendicular view of a general GB using different criteria for the definition of GB atoms a) medium range order b) positional disorder c) excess energy; d) View along the GB plane showing coherence across the GB (grey: fcc atoms, green: other-12 coordinated atoms, blue: non-12 coordinated atoms).

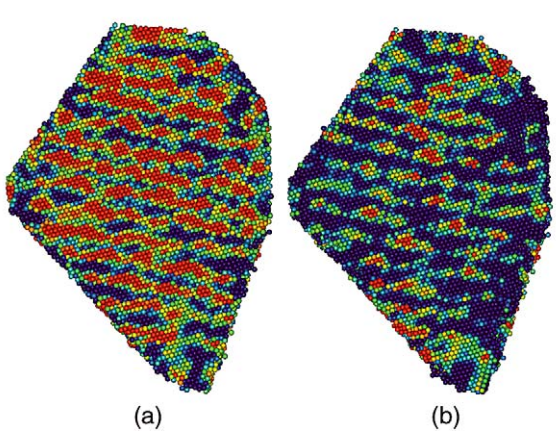

Fig. 5. View normal to the same GB plane as in Fig. 4 showing the local pressure variations (colour code ranges from red = 2 GPa and blue = −2 GPa) a) before deformation b) after 0.5 nsec tensile deformation corresponding to 3% total strain.

4. Mechanical properties of nanocrystalline metals and alloys

4.1. Yield strength and tensile elongation

The mechanical properties of fully-dense fcc metals (Cu, Ni and Pd) with grain size less than 100 nm have been primarily derived from uniaxial tension/compression tests and micro- or nano-indentation [19,22,31,35,36,40,69,70]. Typically, these nanocrystalline metals exhibit significantly higher yield strength, and reduced tensile elongation relative to their microcrystalline counterparts. Furthermore, hardness and yield strength have been found to increase with decreasing grain size in this regime ($<$ 100 nm) down to at least 15 nm. The reasons for this behavior are still under debate as dislocation sources within grains are not expected to operate at these grain sizes. In addition, there is no documented evidence of dislocation

pile-ups in deformed specimens, and any dislocation activity is primarily believed to originate and terminate at grain boundaries. Furthermore experimental evidence [32,33,71–73] indicates that below a grain size of ~10 nm, strength decreases with further grain refinement (the so-called "inverse Hall-Petch-type" relationship). In this regime, grain boundary sliding and/or Coble creep apparently constitute the dominant deformation modes [72,73]; yet, there appears to be no direct experimental confirmation in the published literature of the operation of these processes.

Results of uniaxial tensile tests reveal several unusual features specific to the deformation of nc-metals with fcc structures. For instance, the tensile elongation at fracture of nc metals is low relative to their conventional mc counterparts [19,35,36,69]. This behavior is often attributed to plastic instability originating from the lack of an effective hardening mechanism and/or internal flaws; this instability manifests itself as either shear bands or through "early" necking, as discussed by Ma [74]. Ebrahimi et al. [22] compared 100-μm thick cold-rolled mc copper with electrodeposited nc-Cu, and concluded that the low tensile elongation to fracture in these thin sheet specimens was a consequence of the early onset of plastic instability causing localized deformation. The observation of *macroscopic* chisel-tip fracture in electrodeposited nc-Ni and nc-Cu [22,36] tensile tests with little tensile elongation to fracture supports the localized deformation hypothesis. In this context, Jia et al. [75] have shown the formation of localized shear bands during compression deformation of nc body centered cubic (*bcc*) Fe at quasi-static strain rates at room temperature; they further noted that the width of the band increased with increasing strain and increasing grain size. Shear bands have also been reported in nc Fe-10%Cu alloy in compression and in tension [76], in nc Pd in compression [77] and in nc Cu in fatigue [78]. Early necking was observed in nc-electrodeposited Ni [35] and it was shown that the shape of the tensile stress-strain curve and tensile elongation were affected by specimen size, with uniform deformation along the gauge section observed in small specimens but not in larger specimens. The observed differences were attributed to microstructural inhomogeneity. Since a number of experimental studies have focused on electrodeposited nc Ni, it is pertinent to recall the results of Robertson and Birnbaum [79] on the effects of hydrogen on deformation and fracture of conventional polycrystalline Ni. They demonstrated that hydrogen decreases the stress required for crack advance and localizes deformation.

In the early stages of permanent deformation, independent of the technique used to produce the nc-Ni or nc-Cu, a strong "work hardening" response is always observed [19,22,31,35,36,69] and in some cases, it appears to be stronger than that seen in mc metals [19,22]. Mechanisms for high work hardening in fcc metals include the formation of dislocation locks such as the Lomer-Cottrell locks, formation of dipoles and significant pinning due to dislocation intersections [80,81], none of which has been experimentally demonstrated for nc metals. The inability to observe these features has raised questions regarding the origin of the non-linear portion of the stress-strain curves obtained for nc metals.

The above discussion has focused on fcc metals and alloy. However, mechanical properties of nc body centered cubic (bcc) and hexagonal close packed (hcp) metals and alloys have also been obtained [75,76,82–85]. Electrodeposited nc-Co, for example, with an average grain size of 12 nm shows tensile elongation comparable to that of mc-Co [84]; the limited amount of information available on such systems precludes the extraction of general trends.

4.2. Strain rate effects in tension, compression and indentation

Experimental studies have shown that nc metals exhibit highly strain-rate sensitive mechanical response under different loading conditions. These investigations also reveal that an increase in the loading rate generally leads to an increase in tensile strength, whereas the observed dependence of ductility on loading rate appears to depend strongly on processing, composition and testing method employed to probe rate sensitivity. In an early study published on this topic, Wang et al. [86] found electrodeposited nc Ni to be highly strain

rate sensitive at room temperature. Lu et al. [6,31] reported that electrodeposited nc copper, with an average grain size of about 30 nm, showed only a moderate increase in flow stress, from about 85–150 MPa at 1% plastic strain, as the strain rate was raised from 6×10^{-5} to 1.8×10^{3} s^{-1}. However, the strain to failure was observed to increase markedly with increasing strain rate. This trend is distinctly different from that of conventional mc copper where the fracture strain is known to drop slightly with strain rate. Dalla Torre et al. [35], on the other hand, observed that the ductility of electrodeposited nc Ni decreased as the strain rate was raised from 5.5×10^{-5} to 5.5×10^{-2} s^{-1}. They also found that the tensile strength was essentially independent of strain rate over this range, whereas it increased significantly as the strain rate was raised from 10^{1} to 10^{3} s^{-1}. Mukai et al. [87] investigated the response under quasi-static tension and high-strain-rate dynamic tension (using the split-Hopkinson bar) of several Al-Fe alloys (in the Fe composition range 1.15–1.71 at.%) produced by e-beam deposition. These alloys comprised microcrystallites with high angle boundaries and nc subgrains. The flow stress was found to be higher for the strain rate of 1.1×10^{3} s^{-1} than that for 10^{-3} s^{-1}, although the elastic limit and tensile strain to failure were essentially unaffected by strain rate. Mukai et al. [87] observed that while the high angle boundaries had the effect of enhancing ductility, the smaller grains imparted a higher strength.

A number of complications arise in establishing a clean comparison of the foregoing experimental data. Firstly, the materials with which strain rate effects were studied were produced by different processing routes. Consequently, their structure, purity and distribution of grain sizes were different, and in many cases, the materials were not thoroughly characterized by recourse to high-resolution electron microscopy. Secondly, experimental methods used to impose different strain rates on the specimen often involved widely different loading methods, even in the same study. For example, direct quasi-static tension test results for slow strain rates are often compared with high-strain-rate experiments performed using dynamic loads where the specimen geometry and stress state are considerably different. As a result, it is often difficult to isolate the effects of experimental artifacts from intrinsic rate sensitivity of material response. Thirdly, the volume of material sampled by different experimental techniques is usually different, and given the small specimen dimensions commonly used to probe many nc metals, it is essential to isolate any possible effects of specimen size from intrinsic material properties. With these considerations in mind, Schwaiger et al. [88] performed systematic experiments to investigate the rate sensitivity of deformation of a well characterized, fully dense, nc pure Ni produced by electrodeposition with a grain size of approximately 40 nm (whose structure is revealed at high resolution in Fig. 3(a) and (b)) using two different experimental techniques: depth-sensing instrumented indentation and direct tensile testing. In order to assess the effects of grain size on rate sensitivity, they also performed parallel experiments on a similarly produced electrodeposited ufc Ni.

Fig. 6(a) shows results of constant strain rate indentation tests on the nc Ni at three different strain rates, whereas Fig. 6(b) shows results of four different constant load rates on the indentation response of the same material [88]. It is evident that, over the range of values examined, an increase in strain/loading rate causes a small, but experimentally reproducible, increase in the indentation stiffness which is reflected in the measured hardness values. Identical experiments performed on the electrodeposited, ufc Ni, with an average grain size about 300 nm, did not reveal any rate sensitivity of indentation response or hardness [88]. Considerably larger experimental scatter was observed in the case of the ufc Ni, possibly as a consequence of the significantly larger variation in the distribution of grain sizes. The results summarized in Fig. 6, along with the related data presented in [88], clearly show that nc pure metals exhibit a noticeably more pronounced strain rate sensitivity compared to their larger-grained counterparts.

Fig. 7(a) is a plot of the effect of strain rate, in the range 3×10^{-3} to 3×10^{-1} s^{-1}, for the nc Ni subjected to direct tension loading [88]. It is evident from this plot that the overall trends seen in the indentation tests are also observed in the tensile tests. The flow stress of nc Ni increases noticeably

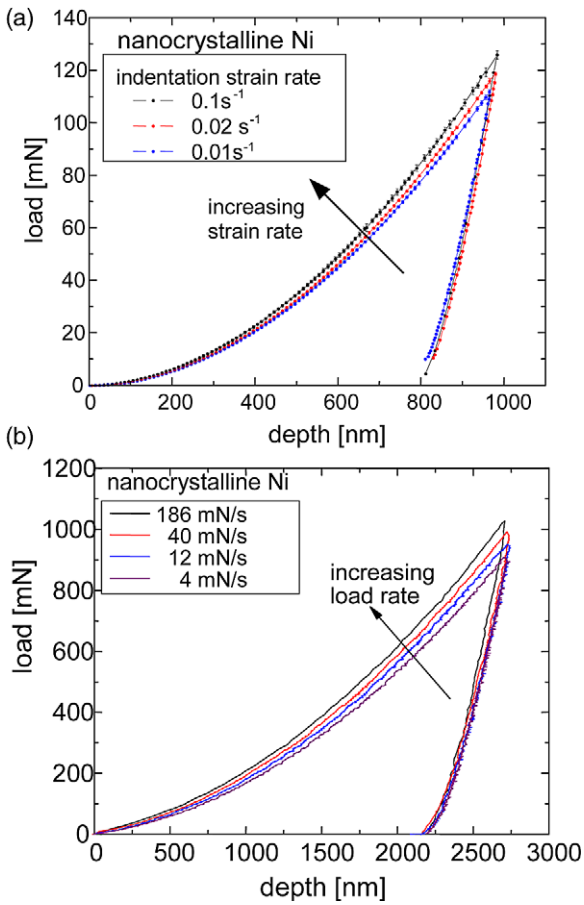

Fig. 6. Depth-sensing instrumented nanoindentation response of electrodeposited nanocrystalline Ni subjected to (a) constant strain rate indentation and (b) constant loading rate indentation. Each curve in (a) and (b) represents an average of 5 different experiments along with an error bar. From Schwaiger et al. [88].

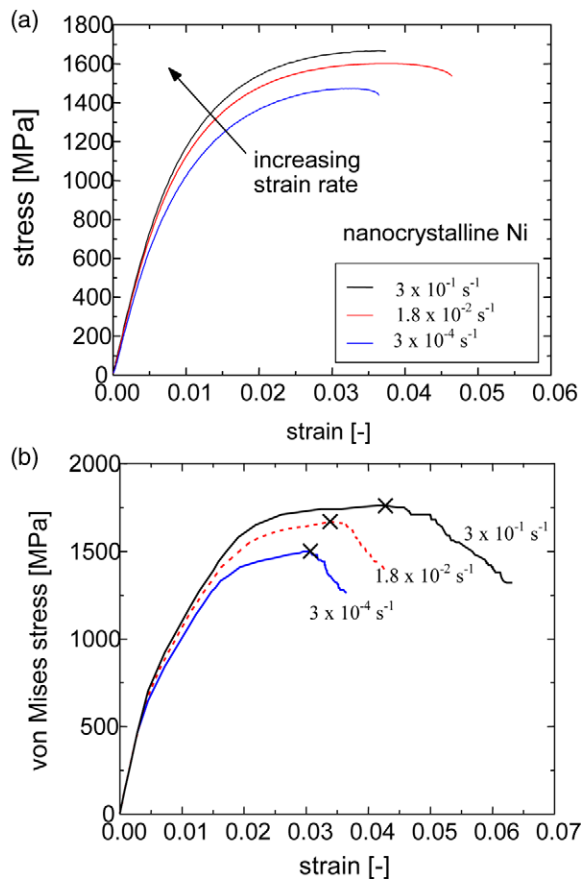

Fig. 7. (a) Results of tensile tests at three different strain rates on electrodeposited nanocrystalline Ni with an average grain size of 40 nm, and (b) Finite element computational simulations of the tensile stress-strain response of nanocrystalline Ni (grain size, 30–40 nm) at three different strain rates, assuming a GBAZ volume fraction of 25%. The symbol "x' refers to tensile strength. From Schwaiger et al. [88].

with strain rate although no clear trends could be established on the effects of strain rate on tensile strain to failure.

The mechanisms underlying the unusual rate-sensitivity of deformation of nc metals and alloys are not fully understood at this time. However, potentially useful insights into such mechanisms can be gained from computational simulations that seek to explore the effects of different structural factors. While such simulations inevitably call for methods that appropriately account for the atomistics of deformation (see later section), continuum formulations of the overall deformation response also provide additional information on rate-sensitivity at realistic time scales which cannot be obtained solely from experiments or atomistic simulations. One such analysis was presented by Schwaiger et al. [88] who employed finite element modeling within the context of unit cell formulations with periodic boundary conditions in an attempt address the following questions. (1) If one postulates the existence of a region neighboring the grain boundary (so called "grain boundary affected zone" or GBAZ) of a nc metal wherein the crystalline lattice is locally strained differently than the interior of the grain, can possible differences between the rate sensitivity of deformation (as esti-

mated, for example, by a pure power law, rate-dependent constitutive response) of GBAZ and grain interior be used to rationalize the overall strain-rate sensitivity of the nanocrystalline metal? (2) How does the volume fraction of such a postulated GBAZ affect deformation? (3) By invoking a criterion for tensile failure within the context of a finite element model, can the overall tensile ductility of the nc metal be estimated as a function of imposed strain rate?

Schwaiger et al. [88] considered hexagonal grains with a plastically softer GBAZ whose deformation was rate-sensitive and a plastically harder grain interior, with the effects of their relative volume fractions on strength and ductility examined for different nc metals. A simple strain-based criterion for failure was postulated: material damage/failure initiates when the local plastic strain reaches a critical value, and the material strength declines linearly with plastic strain to zero over a certain plastic strain increment. This model was used to rationalize stress-strain characteristics and tensile strain to failure as a function of several different strain rates. Fig. 7(b) shows the computationally predicted tensile stress-strain response and tensile strain to failure values for nc Ni (grain size 30–40 nm) at three different strain rates [88], assuming 25 vol.% for GBAZ. While the simple finite element analysis based on the GBAZ unit cell model is at present based on a hypothetical structure which has not been backed by direct experimental verification, it is evident from Fig. 7(b) that it provides one possible rationale for the influence of strain rate on tensile strength and ductility.

Fig. 8 provides a summary of experimental results available in the literature on the effects of strain rate, from 10^{-5} to 10^{4} s^{-1}, on the yield strength of a wide variety of mc, ufc and nc metals and alloys [87]. It is evident from this figure that nc metals show a significantly more pronounced strain-rate sensitivity than coarser grained materials over a wide range of strain rates.

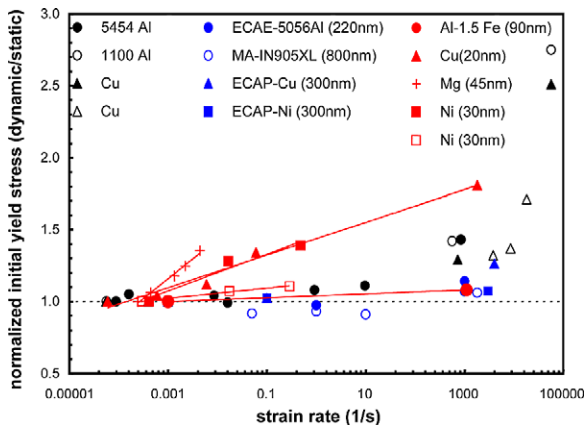

Fig. 8. A summary of experimental data available in the literature on the variation of dynamic yield strength (normalized by the corresponding static yield strength at the slowest strain rate) for a wide variety of microcrystalline, ultrafine crystalline and nanocrystalline metals and alloys. Results taken from literature survey by Mukai et al. [87] (where further information on the original sources can be found), with additional results from Schwaiger et al. [88].

4.3. Fracture and fatigue response

Developing an understanding of the damage tolerance of nc metals and alloys is essential for evaluating their overall usefulness as structural materials or coatings in engineering components. Such understanding should inevitably include comprehensive knowledge of the resistance to fracture initiation and growth under quasi-static and dynamic loading conditions, and of stress- and strain-based total fatigue life and subcritical crack growth under fluctuating loads at different mean stress, cyclic frequency and environment. Many attractive features of nc metals, such as high strength, high hardness, and improved resistance to wear and corrosion damage (as compared to conventional metals), would likely be rendered nonviable if the damage tolerance of these materials does not meet certain minimum acceptable levels for particular applications.

Despite such need, very little published information is presently available on the damage tolerance characteristics of nc metals and alloys. This paucity of information can be attributed to the fact that processing methods, such as electrodeposition or e-beam deposition, which are used to produce fully dense nc materials with uniform purity and uniformly small grain sizes (typically smaller than 100 nm or so) typically yield only thin foils that are at most only several hundred micrometers in thickness. Although these methods can provide

material with large in-plane dimensions, typically in excess of 100 × 100 mm, the small specimen thickness poses considerable experimental difficulties in performing a "valid" test to extract fracture toughness, resistance-curve or fatigue properties. Such difficulties include severe constraints in gripping the test specimen or imposing controlled loads and stress states without experimental artifacts such as out-of-plane bending or buckling of the specimen. Specifically, special precautions should be taken to ensure that the thin foils are not subjected to any bending moments during the application of static or cyclic tensile loads; these measures invariably restrict the range of loads, stress intensity factors, mean stress levels, cyclic frequencies or test environments imposed on the specimen. Similarly, the possibility of buckling of the thin specimen restricts cyclic loading tests primarily to direct tension loading or three or four point bending tests. In addition, a significant range of the subcritical crack growth experiments performed under quasi-static or cyclic loading represent plane stress states because the plastic zone size at the tip of the crack is comparable to or larger than the specimen thickness.

The limited through-thickness dimension of the specimens is an impediment to extracting "valid" damage tolerance properties of nc materials produced by some processing methods. In other cases, it is possible to circumvent these barriers by adopting processing methods, such as the mechanical alloying/consolidation or the equal-channel angle pressing techniques described earlier in Section 2. These methods provide materials of sufficient volume to perform conventional fracture and fatigue tests on nc materials which conform to the standards specified by the American Society for Testing and Materials and which can also be directly compared with results available in the literature on mc materials. A significant drawback of such processing methods, however, is that they produce highly inhomogenous microstructures with pronounced variations in grain size, grain structure, and defect density, and that they contain high initial defect densities as well as relatively large grain dimensions (typically on the order of up to several hundred nm). These complexities constitute serious obstacles in using such materials for studying fundamental mechanisms of crack initiation and propagation and for examining, in a systematic manner, the connections between structure and damage tolerance.

Mirshams et al. [89] studied the quasi-static fracture toughness of thin sheets of nc nickel produced by electrodeposition by investigating their R-curve response. In this approach, the stress intensity factor or strain energy release rate is plotted against the increment in crack length with the objective of assessing the resistance of the material to quasi-static crack growth in a subcritical manner, usually for specimens in a state of plane stress. Mirshams et al. [89] studied subcritical growth resistance by monitoring R-curves with small compact tension specimens where a clip gage was used to monitor crack extension along with optical microscopy. Their results revealed a strong influence of annealing temperature and carbon doping on the resistance-curve behavior of nickel with an average grain size which varied in the range of 19–48 nm. For undoped and 500-ppm carbon-doped nc Ni with an average grain size of approximately 20 nm, they reported plane stress steady-state quasi-static fracture toughness values of about 120 and 20 MPa$\sqrt{m}$, respectively, for specimen thicknesses of 0.22 and 0.35 mm, respectively (with in-plane dimensions being 32 × 40 mm in both cases). By contrast, the corresponding fracture toughness for a pure polycrystalline Ni with an average grain size of 21 μm was found to be approximately 60 MPa$\sqrt{m}$. Thermal annealing and carbon doping were found to deteriorate crack growth resistance. These experiments [89] provide useful insights into the damage tolerance response of the nc Ni. However, they also raise interesting questions and concerns that require substantial further inquiry. (a) The structure of the materials studied had not been investigated in detail using electron microscopy. (b) It appears that small-scale yielding conditions did not prevail over the full range of stress intensity factor values for which damage tolerance values were reported. As a result, the validity in the use of stress intensity factor to characterize fracture response becomes somewhat questionable, especially at the higher stress intensity levels. (c) The reported fracture properties have not been substantiated by independent experimental results

employing different specimen geometry or loading methods. (d) No mechanistic investigations of the origins of differences between different test conditions were undertaken. (e) Typical scatter in the experimental data and issues associated with reproducibility of results for the testing conditions as well as for crack growth monitoring were not reported.

Independent experimental studies of fracture resistance in fatigue-pre-cracked 100 μm-thick pure Ni sheets with a narrow range of grain size (20–40 nm), also produced by electrodeposition, reveal that the plane stress fracture toughness in laboratory air is at least about 25 MPa$\sqrt{m}$ [90]. Thus, the limited extent of experimental information available to date, primarily on electrodeposited nc Ni, appears to indicate that the material has a reasonable fracture toughness considering its relatively high strength and low ductility compared to mc Ni. However, further experimental studies of fracture toughness in nc metals and alloys are critically needed so as to develop a fundamental framework with which their fracture mechanisms can be systematically assessed.

It is widely recognized from the wealth of experimental information available in the literature (e.g., [91]) on conventional metals and alloys that grain refinement markedly influences the resistance to fatigue crack initiation and propagation. In mc materials, a reduction in grain size generally results in an elevation in strength which engenders an increase in fatigue endurance limit during stress-controlled cyclic loading of initially smooth-surfaced laboratory specimens. Since the total fatigue life under such conditions is dominated by crack nucleation and since fatigue cracks generally nucleate at the free surface (in initially flaw-free metals), grain refinement here is considered to result in improvements in fatigue life as well as endurance limit, with all other structural factors set aside. On the other hand, a coarser grain structure with lower strength and enhanced ductility generally plays a more beneficial role in the strain-controlled fatigue response of metals and alloys. Here the low cycle fatigue properties generally improve with grain coarsening, with all other structural factors set aside. The situation is somewhat different when the effects of grain size on fatigue crack growth behavior are examined in mc metals and alloys. In the near-threshold regime of fatigue crack growth, where the extent of fatigue crack growth per stress cycle is on the order of a lattice spacing, finer grained materials usually exhibit a relatively faster rate of crack propagation and a lower fatigue threshold stress intensity factor range [91,92]. This trend is at least partially ascribed to the reduced level of fracture surface roughness seen in the finer-grained metal, as the deflections in crack path promoted during crystallographic crack advance are reduced with grain refinement [93]. In addition, any lowering of effective stress intensity factor range due to premature contact between mating crack surface asperities would also be expected to be reduced due to grain refinement [91,93]. It should be noted, however, that it is often difficult to isolate the sole effects of grain size on fatigue response since other structural factors such as precipitate content, size and spatial distribution, stacking fault energy and the attendant equilibrium spacing of partial dislocations, and crystallographic texture, are also known to have an important effect on the fatigue characteristics of mc metals [91].

Although considerable experimental information is available on the fatigue response of metals and alloys with grain size typically larger than 1 μm, little is known about the fatigue characteristics of ufc and nc metals. Several studies have examined the total fatigue life of ultra-fine crystalline metals produced by equal channel angular pressing, where severe plastic deformation was used for grain refinement [94–96]. In these experiments involving metals with average grain sizes of more than a hundred nm, repeated cyclic loading resulted in pronounced cyclic softening and a weakening of the resistance to low cycle fatigue. These trends, however, have also been seen in microcrystalline metals and alloys where, as demonstrated by Feltner and Laird [97], initially soft microstructures (such as those produced after annealing) cyclically harden, and initially hard microstructures (such as those produced by severe cold working) soften as a consequence of the realignment of dislocation networks to a common saturated state of optimal stored elastic strain energy. Similar behavior is seen when the stacking fault energy of the metal is altered by alloying, although lowering of the

stacking fault energy leads to a cyclically hardened state for the initially soft metal than the softened saturated state attained for the initially harder metal. This effect of stacking fault energy has been attributed by Feltner and Laird [97] to the possibility of restricted cross-slip of screw dislocations whose dissociated partials have a larger equilibrium separation because of the lower stacking fault energy. In this case, the reduced propensity for cross slip leads to different final states in the two cases by constraining the ability of dislocations to reorganize into a common final state. The cyclic deformation results presented in [94–96] for ufc metals thus exhibit trends which are consistent with those well established for conventional mc metals. These studies [94–96] have also shown that the total fatigue life of ufc metals is generally enhanced compared to that of their mc counterparts, as reflected in their relatively high fatigue endurance limit values.

To the authors' knowledge, there appears to be only one published report [98] of the fatigue life and fatigue crack growth characteristics of a well-characterized nc metal with a narrow grain size range below the 100 nm level and with full density and high purity. Hanlon et al. [98] compared the stress-life (S-N) fatigue response of a fully dense, electrodeposited nc Ni (grain size in the range 20–40 nm) with that of a similarly produced ufc Ni (grain size in the 300 nm range) and of a conventional mc Ni. They performed fatigue experiments at zero-tension-zero loading (i.e., load ratio, R = ratio of the minimum load to the maximum load of the fatigue cycle = 0) at a cyclic frequency, ν = 1 Hz (sinusoidal waveform) in the nominal laboratory air environment. Fig. 9 shows that grain refinement has a significant effect on the S-N fatigue response of pure Ni. Nanocrystalline Ni has a slightly higher, but reproducible, increase in the tensile stress range needed to achieve a fixed life and in the endurance limit (defined at 2 million fatigue cycles) compared to the ufc Ni. Both nc and ufc conditions have a significantly higher fatigue endurance limit than the mc metal. Hanlon et al. [98] also conducted fatigue crack growth experiments on nc Ni using edge notched specimens that were subjected to cyclic tension at different R ratios. Fig. 10(a) shows the increase in fatigue

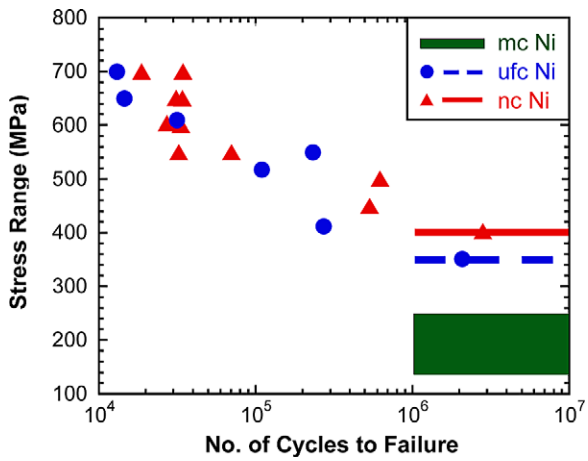

Fig. 9. S-N fatigue response of electrodeposited, fully dense nanocrystalline Ni (grain size 20–40 nm) compared to that of a similarly produced ultrafine crystalline Ni (grain size approximately 300 nm) at $R = 0$ and frequency of 1 Hz in laboratory air environment. Also shown for comparison are the literature values of the range of endurance limit for microcrystalline pure Ni. From Hanlon et al. [98].

crack length as a function of number of constant amplitude fatigue cycles at a common initial stress intensity factor range, $\triangle K = 11.5$ MPa$\sqrt{\text{m}}$, at R = 0.3 and $\nu = 10$ Hz (sinusoidal waveform) in laboratory air for the nc, ufc and mc pure Ni. It is evident that the rate of fatigue crack growth is significantly increased with decreasing grain size in this intermediate regime of fatigue fracture. Fig. 10(b) shows the constant amplitude fatigue crack growth data for pure Ni as a function of grain size from the mc to nc. Again, a marked reduction in grain size from the micrometer to the nanometer scale is seen to result in up to an order of magnitude increase in fatigue crack growth rates in the intermediate regime of fatigue fracture. Such trends are fully consistent with the mechanistic expectations of fatigue fracture based on results available for mc alloys that were mentioned earlier in this section. These results reveal that strategies for grain boundary engineering that lead to an improvement in the total fatigue life may have a concurrent detrimental effect in that they can deteriorate the resistance to subcritical crack growth under constant amplitude fatigue.

The foregoing trends seen in pure nc Ni also appear to carry over to the more complex situation

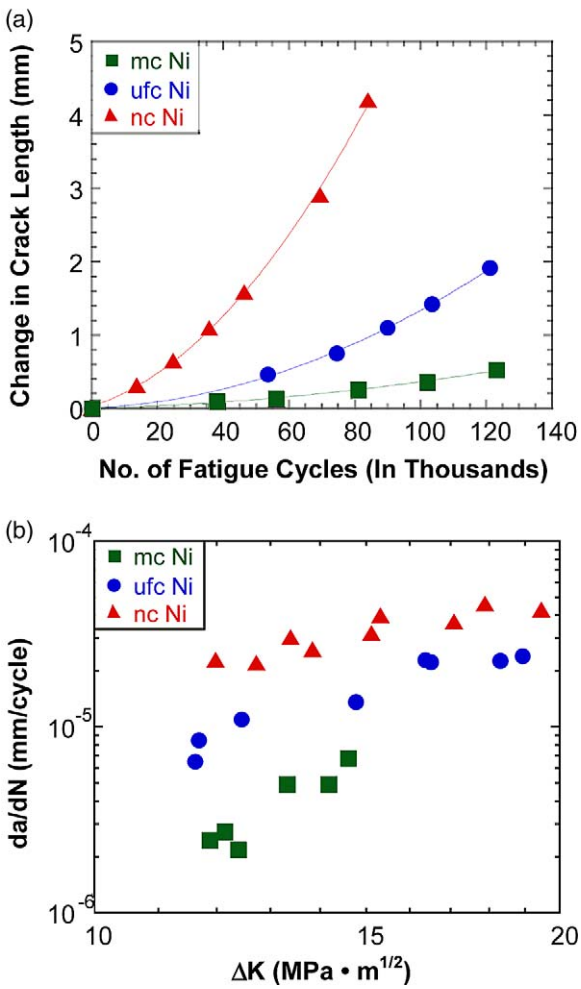

Fig. 10. A comparison of the fatigue crack growth characteristics of pure Ni as a function of grain size spanning the micro- to the nano-scales. (a) Increase in crack length with fatigue cycles for the nc, ufc and mc Ni at a common initial $\triangle K$ = 11.5 MPa$\sqrt{m}^{1/2}$, at R = 0.3 and ν = 10 Hz. (b) Constant amplitude fatigue crack growth response under the same test conditions. From Hanlon et al. [98].

involving commercially produced ufc alloys where conventional fatigue fracture studies could be undertaken using standard experimental techniques widely used for mc metals because of the large volume of material available for investigation. Fig. 11 shows the constant amplitude fatigue crack growth response of a cryomilled Al-7.5 wt% Mg alloy with an equiaxed grain size of approximately 300 nm [99]. Note that, when compared to the

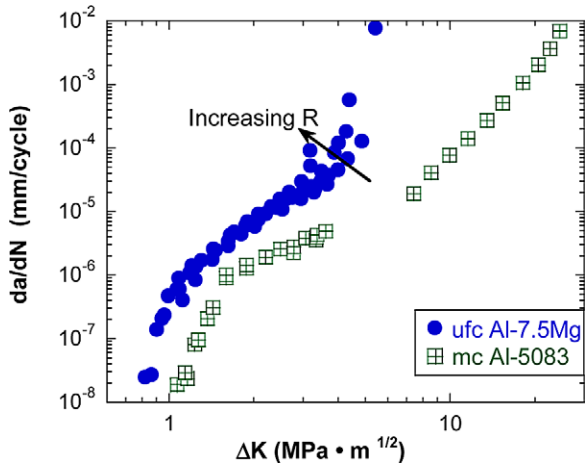

Fig. 11. Comparison of the constant amplitude fatigue crack growth characteristics of a mechanically alloyed Al-7.5 wt% Mg alloy with an average grain size of approximately 300 nm, produced by cryomilling and consolidation, with that of a commercial Al-5083 alloy with microcrystallites. From Hanlon et al. [98].

fatigue crack growth response of a commercial aluminum alloy 5083 with similar composition but with mc structure, the cryomilled alloy shows relatively faster crack growth rates which are more than an order of magnitude higher in the intermediate regime of fatigue crack growth. The finer grained alloy also has a lower fatigue crack growth threshold stress intensity factor range [99].

5. Deformation mechanisms

It was noted in earlier sections that nc metals and alloys exhibit a number of apparent anomalies in their deformation and failure processes as compared to microcrystalline alloys. (1) At grain sizes typically smaller than 100 nm, nc metals seldom follow “Hall-Petch” type strengthening with grain refinement. Such behavior is not fully surprising in that the mechanism commonly associated with Hall-Petch type strengthening, i.e. dislocation pile-up at grain boundaries, has not been experimentally documented in nc metals. Furthermore, below a certain transition grain size, typically on the order of 5–15 nm in fcc metals, there appears to exist a region in which strength and hardness decrease

with decreasing grain size. (2) As shown in Figs. 6–8, the dependence of yield strength on strain rate is distinctly different for nc metals and alloys compared to their mc counterparts. Furthermore, the strain to failure in nc metals appears to vary with strain rate in a manner opposite to that seen mc metals and alloys (see Fig. 7). In this section we review current understanding of deformation of nc metals and alloys, starting with the insights afforded by atomistic computer simulations which are supplemented with experimental observations. The discussion of experimental observations is divided into two subsections: the first dealing with controlled, model experiments, and the second involving microscopy.

5.1. Atomistic simulations

The use of large scale molecular dynamics (MD) simulations has provided insight into the atomic scale processes that may occur during plastic deformation. Such computer simulations are usually performed in uniaxial tension, with high loads chosen to produce a measurable strain within the sub-nanosecond MD time scale. The restricted time-scale, nanoseconds compared to hundreds of seconds in real experiments, may exclude certain time-dependent processes. Simulations should therefore be regarded only as a source of inspiration and quantitative guidance and not as a means to validate or disprove the existence of a mechanism.

Two approaches have been taken in the simulations of deformation: the first where a constant load is applied and the evolution of deformation over time is followed [61,62,100–108], and the second, where deformation is applied by constant strain steps, followed by a short relaxation time, mimicking constant strain rate deformation [59,109]. In both types of simulation, the samples deform at very high strain rates and care should be taken to ensure that the stress waves travel at speeds several orders of magnitude below that of the speed of sound in the sample. This can be avoided by keeping the strain rate on the order of 10^7/sec. Simulations have been performed at room temperature and at higher temperatures [102,110], the latter in order to enhance diffusional activities.

At room temperature and in fully 3D GB networks with a mean grain size below 30 nm in Ni and Cu, the simulation demonstrates the ability of the nano-sized GB network to accommodate an external applied stress by means of GB sliding and emission of partial dislocations involving local structural changes in the network [59,101–103,109]. The interplay between the two mechanisms constitutes the origin of the formation of local shear planes which facilitates further plastic deformation [105]. It has also been observed that along the shear plane, grains with small misorientations can coalesce to form a larger grain. The partial dislocation activity seems to be more effective in grains with a mean grain size that exceeds 10 nm, the size being dependent on the stacking fault energy of the material [100]. When a constant strain rate is applied to nc Cu, the yield stress is found to decrease with decreasing grain size, thereby suggesting a reverse Hall-Petch type relationship [59,109]. This softening has been ascribed to the increased content in GB atoms that facilitate sliding, but no direct link with dislocation activity has been made. Simulations on samples containing 125 grains allowing cooperative grain mechanism have shown that partial dislocations emitted from GBs are also observed in 6 nm sized grains as a means for transferring slip along a mesoscopic shear plane [105].

Both grain boundary and the dislocation plasticity appear to be triggered by atomic shuffling and, to a minor extent, by stress-assisted free volume migration. The result is a local change in the structure of the GB which causes redistribution of peak values of shear stress and compressive hydrostatic pressure in neighbouring parts of the GB network. Atomic shuffling involves short-range atomic motion in which an atom shifts from a position associated with one grain orientation to a position associated with another neighbouring grain orientation or an intermediate one [111]. This process does not involve long-range mass transport and is therefore not diffusion-based. The free volume migration is often observed in connection with partial dislocation emission from the GBs [102,103]. No preferred direction has been observed in the free volume migration as would be expected from a Coble creep mechanism at room

temperature. The changes in local stress distributions during sliding are shown in Fig. 5 where a view perpendicular to the GB plane is given for a GB with a misorientation of 50° around the [110] axis of one of the grains (as was described earlier in the section on grain boundary structure). Fig. 5(a) shows the stress distribution prior to deformation and Fig. 5(b) after 0.5 ns of tensile deformation. This GB has been observed to migrate during sliding (which as shown in Section 5.2, also has some experimental support from bubble raft model studies) and involves atomic activity and, to a minor extent, free volume migration. In other words, the simulations underscore the benefit of the presence of GBs that can reduce their stress state during the deformation.

Fig. 12 represents the atomic configuration of a section of grains 12 and 13 (denoted G12 and G13) in a 12 nm Ni sample, both before (a) and after (b) the emission of a partial dislocation at about 0.3 ns of deformation. The GB and the two neighbouring triple junctions are represented by the blue-green atoms, the hexagonal close packed (hcp) atoms in the stacking fault behind the partial

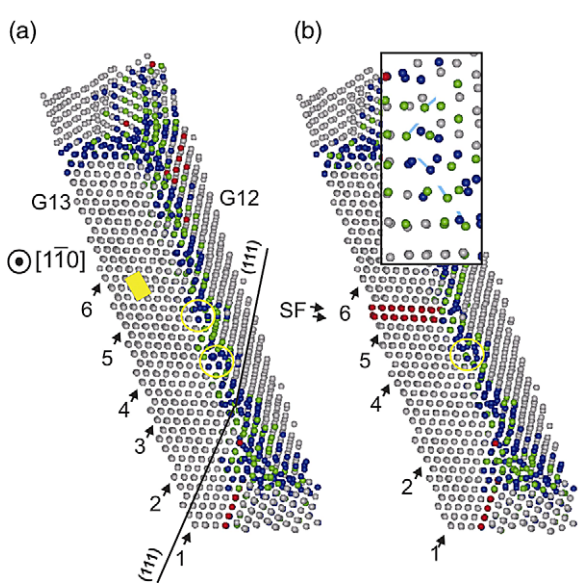

Fig. 12. Section of the GB between grain 12 (G12) and grain 13 (G13) before (a) and after (b) the emission of a partial dislocation. The GB planes where GB dislocations can be observed are numbered. The inset shows a detailed view on the atomic motion towards the nucleation site.

are colored red. The view is along a [1–10] direction of grain 13, where for this grain the unit cell has been highlighted by the yellow rectangle. The grain boundary plane is close to a (1–113) plane of grain 13 and the tilt angle between the observed (111) planes in grain 13 and 12 is approximately 24°. The twist angle was found to be approximately 18°. The GB structure accommodates the above-mentioned misfit through a GB dislocation (GBD) network. The planes where GBD are observed are numbered in Fig. 12(a) and two of them are marked by a yellow circle. Just after the emission of the partial, a free volume unit of the size of a vacancy migrated from GBD3 towards GBD2, followed by a rearrangement of the other GBDs. The migration of atoms towards the nucleation site (free volume away from nucleation site) is shown in the inset in Fig. 12(b). For a more detailed description of the emission process, the reader is referred to [102,103].

Simulations of tensile deformation have also been performed at room temperature on Al with 2D-columnar GB networks. The four columnar-grains have special orientations, so that only three types of grain boundaries are represented [61,62,112]. For a 20 nm columnar diameter sample, it was shown that by increasing the load from 2–2.3 GPa, the strain rate increases by more than two orders of magnitude resulting in strain rates of ~10^8–10^9/s, and that the deformation process changes from one involving GB processes to one dominated by partial dislocations with a strain rate that depends inversely on the grain size. The presence of two length scales, one the grain size and the other represented by the dislocation splitting distance under stress, was recognized [62] as being important to the onset of slip-deformation processes in nc Al. This analysis led to the generation of a “dislocation-nucleation phase diagram” that captured the interplay between these two length scales. Twinning was shown to occur after approximately 12% plastic strain and a stress level of 2.5 GPa for a grain size of 45 nm, with twins originating at grain boundaries as well as in the grain interior from the interactions of stacking faults [112]. The inverse dependence of the strain rate on the grain size has however been recognized as a geometrical consequence of the simulation

setup and the nc-structure. This is so because the strain arising from the nucleation and propagation of a dislocation has a limiting length scale equal to that of the grain size [104]. The observation of a dislocation-dominated regime characterized by mechanical twinning and unit dislocations (at the larger grain sizes) was attributed to the relatively high intrinsic stacking fault (SF) energy for Al potential used in the simulations. The value of the SF energy used in their potential is, however, lower than value for the potential used in the simulations for Ni [63], and therefore the observation of full dislocations cannot be assigned to the stacking fault energy alone.

In a detailed temporal and spatial analysis of the contributions to the excess energy during emission and propagation of a partial dislocation in a 3D nc network, the effective SF energy of the sub-system is found to be reduced by up to 50% via stress relief within the entire grain and structural relaxation of the surrounding GB [63,67]. For a trailing partial to follow its leading partial, and thus for a full dislocation to be observed, the sequence of nucleation and propagation associated with GB structural activity must be repeated. It has been observed that nucleation and emission of a partial corresponds to the removal of a GBD from the GB nucleation site and a reorganization of the remaining GBDs [102,103], suggesting that the barrier for a full dislocation event may be considerable. The atomic activity that underlies the structural relaxation is, to a great extent, inhibited in 2D columnar networks due to the constraints coming from periodic boundary conditions and the process of nucleation and emission is expected to be different [63,67], possibly leading to the observation of full dislocations at smaller grain sizes. That this atomic activity in 3D GB networks is playing a key role in the emission process has also been demonstrated during simulations of nanoindentation of nc-Au [113]. Indeed, by keeping the force constant under the indenter and inhibiting accommodation by means of atomic activity, full dislocations are emitted under the indenter, propagating through the grain until they are absorbed at opposite GBs. It is important to realize that due to the sub nanosecond time restrictions of an MD simulation (usually less then 0.5 ns), the emission of a second partial on the same or on an adjacent plane, and therefore the removal of a stacking fault defect or the creation of a twin might not be seen. Much longer simulations times might be required for this phenomenon to be actually observed [63,67].

Deformation studies at higher temperatures (0.7–0.9 Tm) suggest a Coble creep mechanism with GB sliding as an accommodation mechanism, known as Lifshitz sliding [46,110]. The conclusion is drawn from calculation of an activation energy extracted from the first 100 ps of strain-time curves performed at different temperatures all above 70% of the absolute melting temperature. Although extrapolations of Coble creep mechanism to room temperature have been proposed [46,110], there does not appear to be justification for such an extrapolation. This is because there is no fundamental basis to assume that the rate-limiting process at a temperature close to the melting temperature, where grain boundaries are no longer stable at the timescale of seconds, can be also the dominant process at room temperature.

Calculations of activation energies from constant load experiments [110] where the strain rates are taken from the very initial stages of deformation can be misleading. Fig. 13 shows a strain-time curve for a nc Ni sample with a mean grain size of 12 nm where the sample is deformed during 1.5 ns. The initial strain rates of 10^7/s steadily decrease by an order of magnitude over the ns range [51]. This effect is expected to increase for increasing deformation temperatures, especially

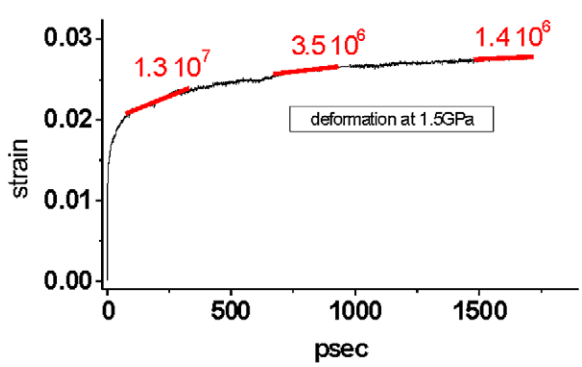

Fig. 13. Strain versus time for a computer simulated nc-Ni sample with mean grain size of 12 nm showing the decrease in strain rate as simulation time continues.

when temperatures are high enough for grain growth. The plot shows that the calculation of activation energies from Arrhenius-type curves will give time-dependent results since a steady state is not reached [101] and that it is therefore inappropriate to draw conclusion from this type of analysis on the type of constitutive law that fits the deformation mechanism, such as establishing a Coble creep dependence. Therefore, the only meaningful information that can be extracted from MD simulations is from a careful classification of the atomic processes taking place during deformation and verifying the occurrence of these processes at the longer nano-second timescale.

Computational models at the atomic level have also been developed in recent years to address the fundamental issue of nucleation and kinetics of defects in response to mechanical loading. In order to make direct correlations with experiments in a quantitative manner, many of these studies [113–118, for example] have focused on defect nucleation under conditions of nanoindentation of surfaces, which is a convenient experimental tool for quantifying local deformation. Using controlled model experiments involving a raft of initially defect-free soap bubbles as a basis to explore defect nucleation and motion in a systematic manner (see the discussion in the next subsection), Li et al. [119] and Van Vliet et al. [120] presented an analytical formulation of the elastic limit which is capable of predicting the location and slip character of a homogeneously nucleated defect in crystalline lattices. By postulating an energy-based local elastic stability criterion, they have extended the formulation to the atomic scale. They have also demonstrated that this approach can be incorporated efficiently into commonly used computational methods such as molecular dynamics and finite element models. They have further validated and calibrated the criterion for defect nucleation in the single crystalline, initially defect-free lattice through nanoindentation experiments on fcc crystals and on the bubble raft model. Quantitative understanding of defect nucleation and motion would be significantly enhanced if such criteria can be extended to include defect nucleation at grain boundaries in nc metals.

5.2. Bubble raft model experiments

As noted in the context of Fig. 1, experimental studies on a number of nc metals have indicated the possibility of a decrease in strength and hardness with decreasing grain size, below a certain transition grain size, which is approximately 10 nm. Mechanistic origins of such an inverse Hall-Petch type effect are not well understood at this time, partly because of the limitations of available experimental tools to image and record, during deformation, the deformation processes at nanometer resolution. In order to overcome such limitations, attempts have recently been made to visualize defect nucleation at the atomic level in nc metals using the Bragg-Nye soap bubble raft model [121], which is a two-dimensional (2-D) analog to fcc metals [122,123]. As reviewed in [123], this method entails the creation of a single crystalline or polycrystalline 2-D raft of up to several hundred thousand uniformly sized soap bubbles by forcing pressurized air through a micropipette in a soap solution. The interactions among the 1-mm diameter bubbles are analogous to the interatomic interactions of fcc metals, with the bubble size having a geometric scaling with the atomic diameter of approximately 0.3 nm. Van Vliet et al [123] produced such polycrystalline rafts with an average grain size that had a value between 4 and 37 nm (based on the above scaling analogy) and a variation in grain size of 20% or less. New rafts were produced for each grain size. Localized deformation was introduced by nanoindentation, and defect nucleation was monitored using video photography. The polycrystalline raft was used to assess whether the deformation mechanisms varied with grain size. The maximum pressure under the indent was then estimated corresponding to the onset of defect activity and was associated with the magnitude of the critical resolved shear stress required to induce defect activity. Fig. 14 shows the variation of the flow stress (normalized by the value of the critical flow stress at the maximum strength at the transition grain size) for defect activity, which approximately correlates with yield strength, as a function of the grain size. Defect activity was identified to be initiated by two different mechanisms: (i) nucleation of discrete dislo-

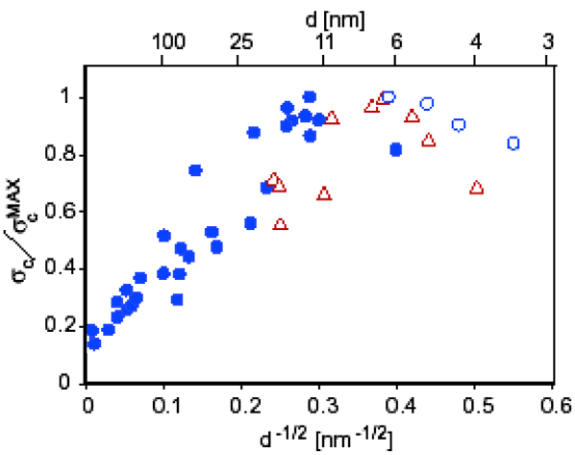

Fig. 14. Normalized critical stress as a function of grain size *d*. Red triangles indicate critical stress to initiate plasticity in bubble raft nanoindentation experiments [123]. Filled and open blue circles indicate experimental data for electrodeposited Ni from several references cited in [123] and molecular dynamics simulations for Cu [59], respectively.

cations at grain boundaries and triple junctions and (ii) motion of grain boundary regions by migration and/or sliding. Crystalline rafts with an average grain size typically larger than 7 nm primarily exhibited the former process whereas the latter mechanism was dominant below an average grain size of about 7 nm. Despite the obvious limitations of the 2-D bubble raft in providing realistic features of defect nucleation in a 3-D nc metal, the results of Fig. 14 provide an experimental justification and a unique in-situ visualization of the possible occurrence of a transition from strengthening with grain refinement to weakening with grain refinement. Remarkably, the transition grain size of approximately 7 nm found in the bubble raft experiments is the range of values found from hardness measurements of nanocrystalline Ni, which are also plotted in Fig. 14. It is also interesting to note that the observations of weakening with decreasing grain size below 7 nm in the bubble raft experiments are qualitatively similar to those predicted by Shiøtz et al. [59] in their atomistic computational simulations of nanocrystalline Cu; these predictions are also indicated in Fig. 14.

5.3. Transmission electron microscopy observations

5.3.1. Dislocation plasticity

It is generally accepted that conventional dislocation sources such as the Frank-Read source cease to operate in nc metals, and that grain boundaries become potential dislocation sources and sinks. Post-deformation observations of nc specimens in the transmission electron microscope have failed to reveal dislocation debris characteristically observed in deformed mc specimens [41,69]. Alternate deformation mechanisms such as grain boundary sliding, Coble creep and grain rotation have been suggested in simulations and proposed in analytical models [72,73,101,109,124,125]. However, convincing experimental evidence has not been provided thus far to support the notion that these mechanisms are operative. Limited creep studies that have been performed to date provide conflicting information: GB sliding is suggested as the deformation mechanism in electrodeposited Cu during tensile creep tests performed at 20–50°C [126], but similar experiments on nc-Cu and nc-Pd show creep rates much lower than that predicted for diffusional creep at low-to-moderate temperatures [127]. Grain boundary sliding has been proposed as a dominant deformation mechanism in nanocrystalline Zn [85] but experiments were conducted at or above room temperature, which is a significant fraction of the homologous temperature of zinc.

The absence of dislocation debris in deformed specimens has led to several in-situ deformation studies in an attempt to observe possible dislocation activity during deformation [41,128–131]. While the in-situ deformation technique is instrumental in revealing deformation processes at the crack tip, the problem associated with the influence of the pair of free surfaces present in the electron-transparent region of the thin foil on inferred deformation modes [132] raises questions about the applicability of these observations to bulk material deformation. However, the observations are intriguing, since in nearly all cases, dislocation activity is observed in the vicinity of the crack tip.

In-situ deformation of a tensile specimen in the transmission electron microscope [41] has revealed

that, in nc Ni with grain size in the 30–40 nm regime, copious dislocation emission is triggered at the crack tip, and that there is some evidence of this process extending over several grains ahead of the tip. Furthermore, it appears that these dislocations are generated at grain boundaries, and that they proceed to the adjacent/opposite boundary where they are absorbed. Nano-scale voids evolve at grain boundaries and triple junctions ahead of the crack tip and they eventually grow and coalesce to form larger dimples. Similar observations have also been made by Youngdahl et al. [129] in nc Cu produced by inert gas condensation followed by compaction. The material was reported as being 97% dense and having a broad grain size distribution range from 20–500 nm, although "the majority" was between 50–80 nm. More recently, in-situ studies have been performed on uniform 100 nm thick Ni films synthesized either by pulsed laser deposition or by DC magnetron sputtering [131]. Both films had grain sizes below 50 nm and were transparent to electrons so that thinning procedures could be avoided. A starter crack was introduced before deformation. The authors report "pervasive dislocation nucleation and motion" in grains as small as 10 nm and indirect evidence for minimal contribution from GB sliding. A different behavior in failure mechanism was observed between the two films, and this was attributed to the presence of GB porosity.

In-situ electron microscopy studies to date have been able to confirm dislocation activity in the neighborhood of a crack tip during tensile testing. There is no evidence of extended partial dislocation activity *during* the in-situ experiments (as suggested by simulations), but this might be due to several reasons: i) the difference in time scales between the in-situ experiments and the simulations as suggested in previous paragraphs, and ii) experimental difficulties relating to the dynamic nature of the in-situ experiments combined with the need to conduct them in the bright field mode at high magnification in order to view the individual grains and dislocations within them. Recent atomistic simulations of crack propagation in nc-Ni samples similar to those reported previously have shown evidence for extensive dislocation activity at the crack tip, including full dislocations and twinning in grains as small as 10 nm [133]. These results indicate that the dislocation activity observed in in-situ tensile testing in the microscope has to be related to the propagation of the crack and that extrapolation to bulk tensile deformation may be tenuous.

Recently, it was inferred from X-ray diffraction experiments that cold rolling of 10–30 nm grain size Pd (produced by gas-phase condensation) caused an increase in stacking fault density, although the grain shape remained equiaxed and there was no preferred texture [30]. Further, in this study [30], transmission electron microscopy evidence was provided for the first time for the existence of a mesoscopic glide plane.

5.3.2. Twinning

Twinning is an alternate mode of plastic deformation and it has been observed in conventional fcc metals and alloys with low stacking fault energy (e.g. austenitic stainless steel [134]; Cu-Al alloys [135]); Twins have also been observed in fcc metals and alloys with relatively high stacking fault energy when extreme deformation conditions are imposed (cryogenic temperatures, shock-loading, and/or large strains). For example, deformation twinning was noted in an Al-4.8% Mg alloy during cryogenic shock loading [136]. Embury et al. [135] postulate two necessary conditions for the formation of deformation twins in fcc metals: (1) a change in the dominant slip system must occur, and (2) a critical stress level needs to be reached locally at the site of the twins. Recently, Kumar et al. [41] reported the observation of twins during the deformation of electrodeposited nc Ni in the transmission electron microscope, (Video images of the formation of twins can be found in the supplementary material provided in [41] at the website: http://ninas.mit.edu/Submission/SupInfo/index2.html). Computer simulations of deformation of nc Al with a grain size of 45 nm [112] have also shown that twinning occurs after approximately 12% plastic strain and a stress level of 2.5 GPa, with twins originating at grain boundaries as well as in the grain interior, the latter resulting from the interactions of stacking faults. Chen et al. [137] have reported deformation twin-

ning in vapor-deposited nc aluminum that was severely deformed by micro-indentation and grinding.

Several key issues should be considered before the possible role of twinning in influencing the deformation characteristics of nc metals and alloys can be ascertained. Growth twins are frequently observed in electrodeposited Ni independent of grain size (Fig. 15(a),(b)), in nc Cu produced by gas-phase condensation (Fig. 11(c)), in ufc vapor-deposited Au (Fig. 15(d)) and in vapor-deposited nc Al [137]. Care must be exercised to differentiate deformation twins from these growth twins. Furthermore, little is known about the role of growth twin boundaries in assisting or hindering plastic deformation in nc metals, and about the interaction of emitted dislocations with the growth twin boundaries. Computations have thus far not included such growth twins in the starting microstructure and since grown-in twins are observed experimentally in very small grains, simulations should address this issue. In the case of conventional mc Ni which is prone to twinning during strain annealing, it has been shown that the presence of twin boundaries enhances corrosion resistance and reduces the propensity for intergranular fracture [138,139]. Hydrogen and other interstitial impurities are often present in electrodeposited materials and these can also influence the twinning stress of the material. For example, it is known that nitrogen lowers the stacking fault energy in stainless steels and encourages twinning [140]. There also remain questions regarding: i) the

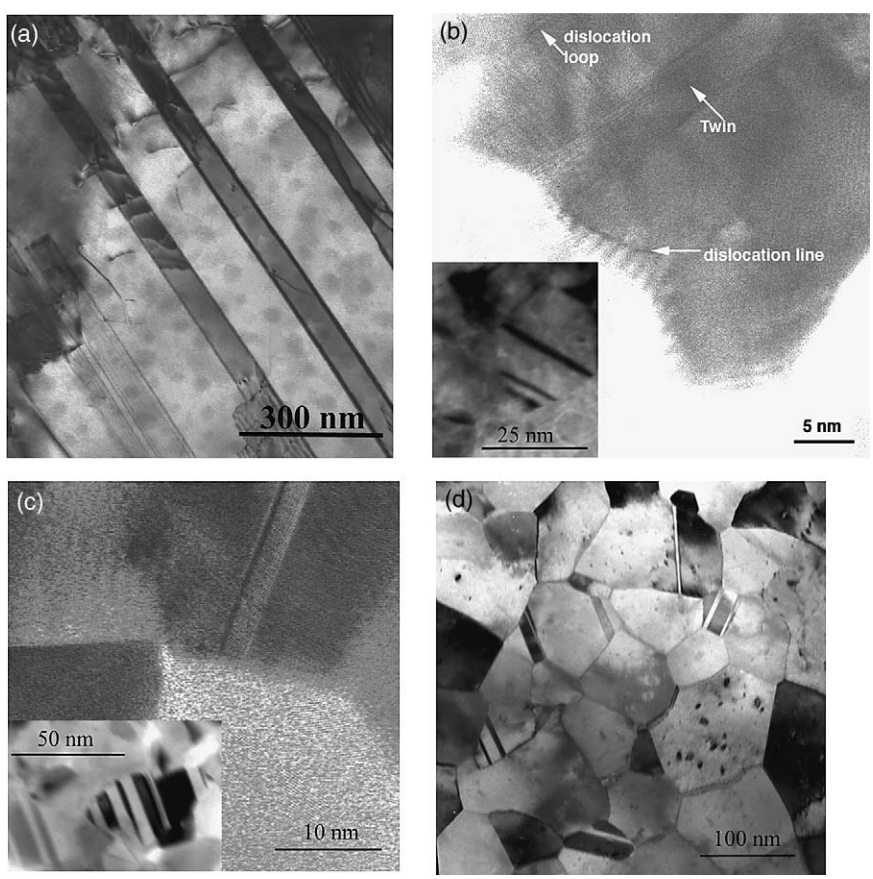

Fig. 15. Growth twins (a) in electrodeposited mc-Ni, (b) in electrodeposited nc-Ni, (c) in nc-Cu produced by gas-phase condensation, and (d) in ufc Au produced by electron beam deposition. Insets in (b) and (c) are bright field images, as are (a) and (d). (b) and (c) are high resolution images.

nucleation mechanism of such deformation twins, ii) the stage of deformation at which they evolve, and the dependence of onset of twinning on grain size, and iii) the role they play in affecting the overall deformation characteristics of the nc metal. Currently available experimental evidence for twinning in nc metals is predicated upon observations made under special circumstances. For example, twinnig in nc Al was observed in a specimen which was subjected to significant plastic deformation by indentation and extensive grinding [137], whereas observations of twinning in nc-Ni were reported during deformation in the transmission electron microscope in the last ligament of a thin foil [41].

In summary, atomistic simulations seem to have a potential for providing insight into the deformation mechanism at the atomic scale. However, many aspects of the proposed mechanisms remain to be explored and the comparison between simulated samples and experimental samples should be considered with the necessary criticism. For instance, simulated samples always have grains without any defects, which is probably justified for some kind of defects in grain sizes below 20 nm, but less probable in 70 nm sized grains, as has been simulated in 2D columnar networks. The incorporation of defects in the larger grains could activate dislocation sources other then GBs and therefore alter the global deformation response. Moreover the simulated samples have densities comparable to full dense nc-materials obtained by electrodeposition or severe plastic deformation, but the experimental samples contain nanovoids, as evidenced by positron lifetime annihilations. The simulated samples contain only free volume units of the size of a vacancy or less.

6. Fracture mechanism(s)

The evolution of damage and final fracture in nc metals and alloys is only beginning to be understood. Few systematic experiments have been conducted to elucidate how these processes proceed. In what follows, we summarize the main experimental findings and their interpretation through simulation and modeling, followed by a critical view of microstructural issues.

The absence of substantial macroscopic tensile ductility in nanocrystalline fcc metals together with the observation of dimpled rupture on fracture surfaces (for example in Ni in [35,41,106]) leads to the hypothesis that deformation is localized. Whereas localized deformation is clearly manifested through the appearance of shear bands on deformed specimen surfaces in nc bcc Fe and Fe alloys even at quasi-static strain rates [75,76], this does not appear to be the case in their fcc counterparts, where shear bands have been reported to occur in nc-Ni only after high strain rate deformation [35]. It is worth noting that with the exception of [35], compression specimens have been typically used to observe shear bands in nc materials and they can be often be deformed to larger strains than possible in uniaxial tension. The restriction to thin sheet geometry for electrodeposited material has precluded compression tests and encouraged widespread use of tension tests for the nc metals produced by this process. In bcc nc-Fe, TEM images taken from within the shear bands show grains that are elongated in the shear direction whereas the grains remain equiaxed outside of the band, a further testament to deformation localization [75]. However, since these tests were done in compression, fracture surface were not available for observation. How the deformation structure evolves inside a shear band requires further experimental investigation.

In-situ TEM studies conducted for the purpose of detecting possible dislocation activity during deformation of nc metals and alloys also provide some insights on the damage evolution process ahead of the crack tip. In electrodeposited nc Ni [41], voids at grain boundaries and triple junctions ahead of the main crack grow with progressive loading. A sequence of observations from [41] is reproduced in Fig. 16(a)–(c) that illustrates damage evolution during deformation. While there is uncertainty about the validity of extending such observations to bulk behavior, MD simulations also suggest the formation of voids at grain boundaries and triple junctions ahead of the main propagating crack which then link up [141] producing intergranular fracture.

In-situ tensile study on DC magnetron sputtered nc-Ni and pulsed laser deposited nc-Ni [131] films

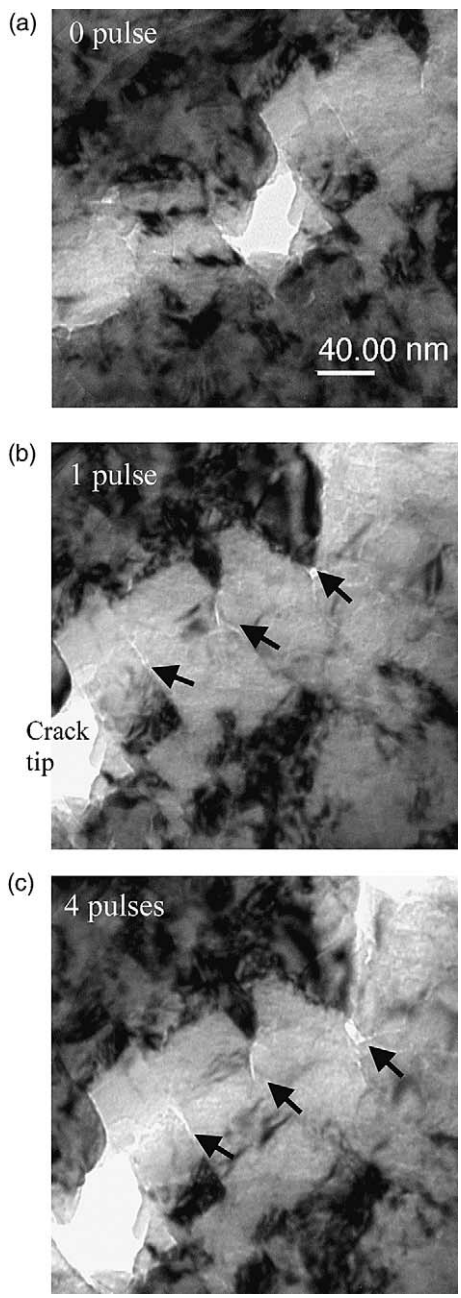

Fig. 16. A region ahead of a crack tip in a thin foil of nc-Ni with 30–40 nm grain size that was subjected to in-situ deformation in the TEM by the application of displacement pulses. In (a), the region is shown in a "reference state" (0 pulse) even though the specimen is under load; in (b) a single additional displacement pulse opens the voids at grain boundaries and triple points; and in (c) the application of 3 additional pulses further opens these voids and promotes cracking along boundaries.

of uniform thickness, both having mean grain sizes of 15–20 nm, revealed the importance of the presence of nano-scale voids in the structure prior to deformation. The magnetron sputtered Ni, containing some grain boundary porosity, failed in a brittle manner via rapid coalescence of intergranular cracks whereas the crack propagated slowly, accompanied by continuous film thinning, in the laser deposited film that contained no porosity

Fracture surfaces resulting from tensile tests have frequently shown dimpled rupture in electrodeposited nc-Ni, nc Al-Fe and nc-Cu [22,35,36,41,87]. Further, it has been shown that the dimple size is significantly larger than the average grain size; in addition, in [41], a pair of mating fracture surfaces was shown that clearly illustrated the presence of significant stretching of the ligaments between the dimples that was taken to be indicative of appreciable local plasticity. An example of a fracture surface obtained from a tensile specimen of electrodeposited nc Ni with a grain size of around 25–30 nm is shown in Fig. 17(a). It reveals dimpled rupture with the dimple diameter and dimple depth (~300–400 nm) being an order of magnitude larger than the grain size (Fig. 17(a)). Furthermore, the dimple size is uniform and extends across most of the specimen cross-section (Fig. 17(b)).

When the grain size is reduced to ~10 nm or less, as in the case of an electrodeposited Ni-W alloy (Fig. 2b), the resulting fracture surface from a tensile specimen still continues to show what appears to be dimpled rupture (Fig. 18(a)) with the important difference that the dimple diameter on an average is finer in size (but still much larger than the grain size) relative to those seen in Fig. 17(a). Whether this is a direct consequence of a reduction in grain size or is influenced by the presence of W in the alloy is unclear. Further, the dimples in Fig. 18(a) are shallower than those in Fig. 17(a), and they exhibit a wide size distribution. A significant portion of the tensile specimen fracture surface exhibited this mode of failure (Fig. 18(b)). In-situ cracking of tensile specimens in the TEM confirmed that the crack propagates in an unstable manner in the nc Ni-W alloy as compared to the 30-nm grain size electrodeposited Ni.

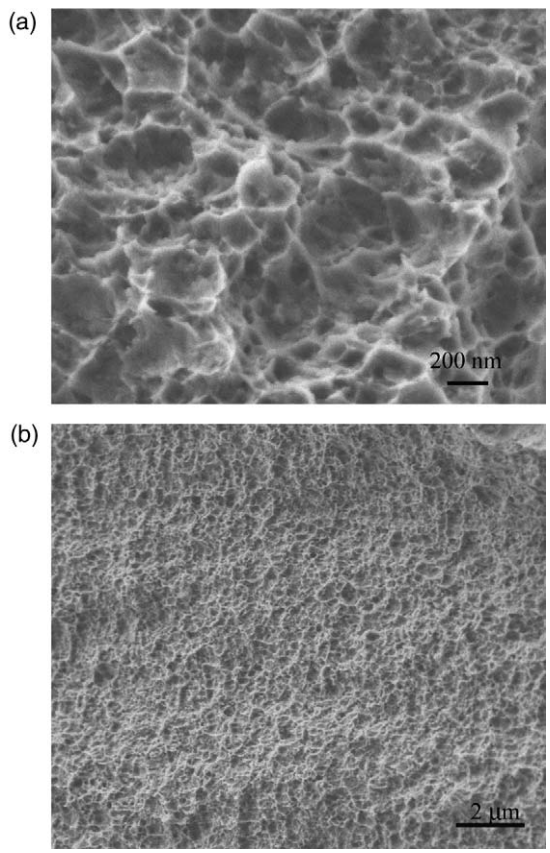

Fig. 17. Fracture surface of a 30 nm grain size electrodeposited Ni tensile specimen that was deformed in-situ in the TEM but was fractured outside the microscope: (a) dimpled rupture with dimples that are significantly larger in diameter (200–400 nm) than the grain size, and (b) a lower magnification image showing the prevalence of the fracture mode.

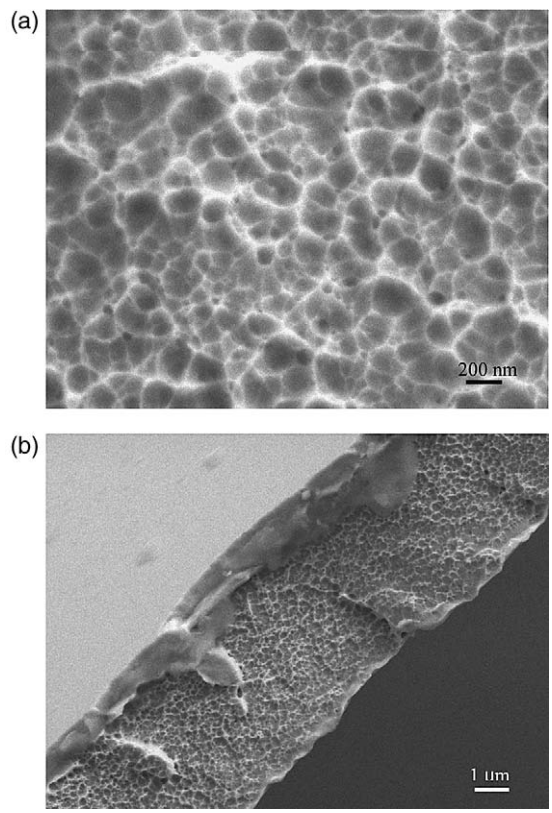

Fig. 18. Fracture surface of a ~10 nm grain size electrodeposited Ni-W tensile specimen that was deformed in-situ in the TEM but was fractured outside the microscope: (a) dimpled rupture with a range of dimple sizes that are larger in diameter (100–200 nm) than the grain size, and (b) a lower magnification image showing large areas of the fracture surface exhibiting this mode of fracture.

As stated above, atomistic simulations of crack propagation in full dense nc-Ni with mean grain sizes of 6 nm and 12 nm [141] have shown that a *preformed crack* propagates intergranularly with the formation of nano-scale voids ahead of the crack. In the simulation, plasticity is only observed in the vicinity of the crack tip and therefore collective events such as those that may occur during tensile deformation are excluded. On the other hand, molecular dynamics simulation of tensile deformation where plasticity is observed in the entire specimen containing 125 grains with a mean grain size of 6 nm shows the formation of mesoscopic shear planes as a result of GB sliding and partial dislocation activity. Additionally it has been demonstrated that due to the presence of special GBs that resist GB sliding, local shear planes can be formed, creating a cluster of grains embedded in a sliding environment [106]. Thus, a plasticity length scale of the order of several grain sizes emerges that may correspond to the dimensions of the dimple structures seen on the fracture surfaces resulting from experiments. In the simulations [106], the applied technique does not allow the observation of fracture, both, due to the time restriction and due to the applied periodic boundary conditions. The formation of such a local network of shear planes could lead to the formation of nano-cavities via unaccommodated GB sliding,

and eventually macroscopic fracture that could be additionally enhanced by the presence of preexisting voids.

Based on the observations of dimpled rupture, dislocation activity at the crack tip, and the formation of voids at grain boundaries and triple junctions in the regions ahead of the advancing crack, Kumar et al. [41] proposed a model for damage evolution and fracture which is captured in the sequence of events schematically depicted in Fig. 19. In the early stages of deformation, dislocations are emitted from grain boundaries under the influence of an applied stress, when intragranular slip is coupled with unaccommodated grain boundary sliding to facilitate void formation at the grain boundaries. Such voids do not necessarily form at every boundary. Triple junction voids and wedge cracks can also result from grain boundary sliding if resulting displacements at the boundary are not accommodated by diffusional or power law creep. These grain boundary and triple junction voids then act as sites for nucleation of the dimples which are significantly larger than the individual grains and the rim of these dimples on the fracture surface do not necessarily coincide with grain boundaries. Thus, at a local level, the nc-Ni demonstrates considerable plasticity (and could represent localized deformation within a shear band). Its deformation and fracture processes are closely related to the coupling of dislocation-mediated plasticity and formation and growth of voids.

The fundamental difference between the two approaches is that the atomistic simulations reveal intergranular crack propagation, where the GBs that are chosen by the crack path are determined by plastic deformation processes, whereas the model illustrated in Fig. 19 proposes the formation of local ligaments with free surfaces as the voids evolve, stretching in concert and finally leading to transgranular fracture. Whatever the fracture mechanism, it is evident that the fracture will be heavily influenced by microstructural features which have up to now been mostly neglected such as the presence of nano-scale voids or even bubbles and the presence of grown-in twins. It is well known that bubbles filled with hydrogen (hydrogen bubbles) are often present in electrodeposited metals and these could serve as nucleation sites for the dimples without the need to nucleate additional voids during deformation [31,142]. These bubbles can be present at GBs as well as in the grain interior. Additionally, positron annihilation has shown the presence of nanovoids of 10–20 vacancies in nearly all nc samples [35,39], and they are considered to populate grain boundaries and triple junctions. However, their location has not been experimentally verified. The presence of twins has been suggested as an interface control mechanism in coarse-grained metals [139] and may represent a relevant microstructural feature that influences fracture, since many of the nc metals contain grown-in twins. The role played by twin boundaries (or boundaries close to twin misorientation) in discouraging GB sliding and thereby determining a plasticity scale that is comparable to experimentally observed dimple size has been suggested in simulations [106].

7. Concluding remarks

Research into the structure, deformation and failure of nanocrystalline metals and alloys has provided a wealth of experimental information during the past decade. Such knowledge forms a critical foundation for the development of newer generations of structural materials whose mechanical properties can be modulated through the judicious design of grain boundaries. Advances in characterization tools and computational simulations have further aided progress in this area, and have provided unprecedented opportunities for interpreting the mechanical deformation mechanisms at the nanoscopic size scales.

In considering the structure of nc metals and alloys and its impact on deformation behavior, the role of grain boundaries is clearly paramount. Experiments and computations have demonstrated that these grain boundaries are substantially similar to those in mc metals and alloys and that there is no “grain boundary region” that is highly disordered or amorphous as originally proposed. However, this is where experimental characterization has stopped. Computations have taken this to the next level of detail and shown the effects of atomic structure at the boundaries (boundary type

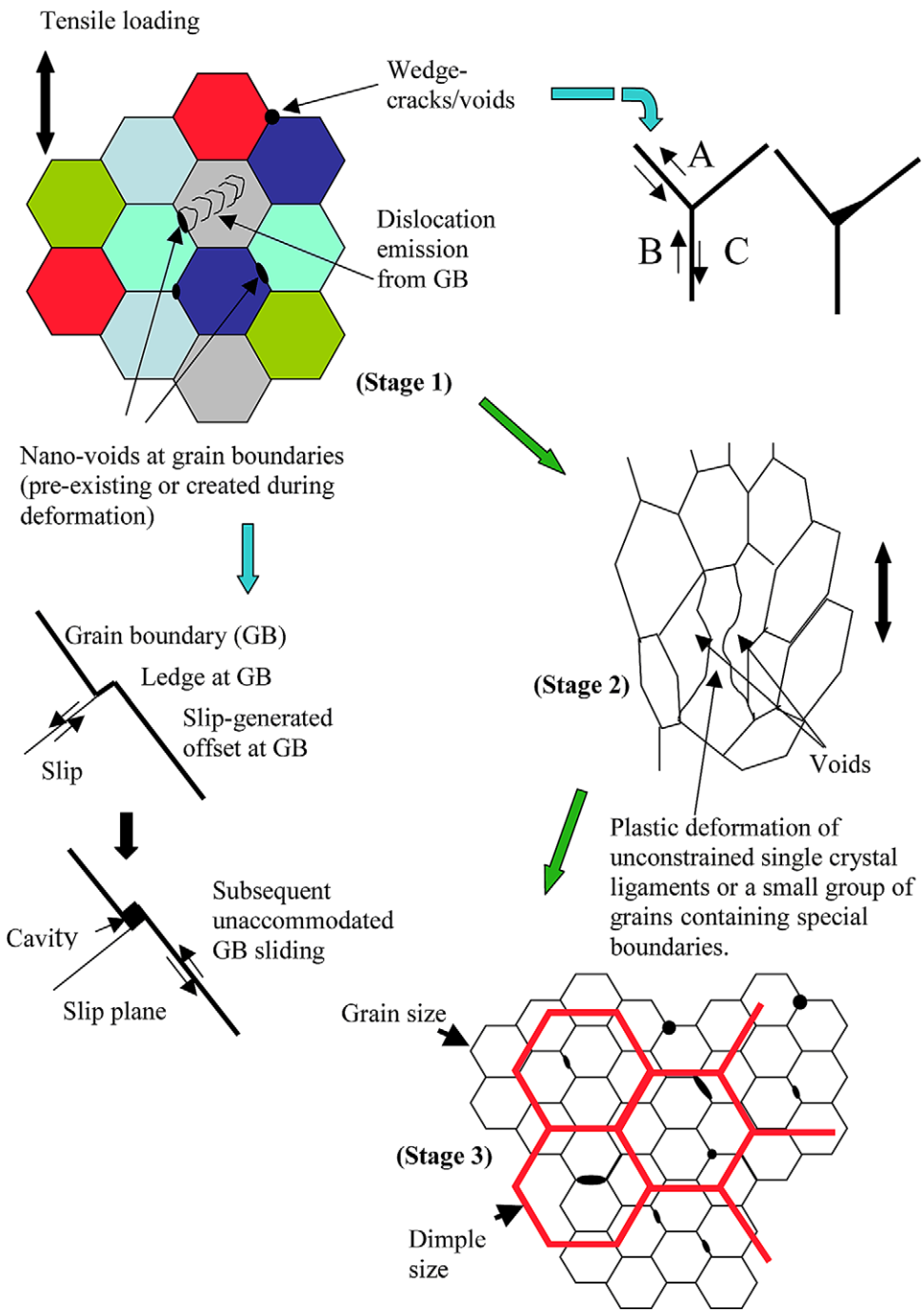

Fig. 19. A schematic illustration depicting how deformation evolves in nanocrystalline nickel based on experimental observations i) during in-situ deformation in the TEM, and ii) of resulting fracture surfaces in the SEM. Dislocation motion, void formation/growth at grain boundaries and triple junctions, the formation of partially unconstrained ligaments that deform plastically, and the interaction of these various features to produce the eventual fracture morphology are all synthesized in this figure.

and boundary stresses—equilibrium versus non-equilibrium) on grain boundary sliding and the capacity of a GB to emit dislocations into a grain and absorb dislocations. While these descriptions seem plausible, there is currently little direct or indirect experimental evidence to support the computational finding even for simple tensile deformation. Clearly, the field would benefit immensely from dedicated experimental efforts on grain boundary structures in nc metals and their response to applied stress. Furthermore, experimental validation of computations is required at a more fundamental level rather than at the level of macroscopic mechanical properties such as hardness, strength and ductility because factors that affect these properties (for example, impurity content, nanoscale porosity, etc) cannot be conveniently incorporated into computations.

Microstructural characterization has also not been systematic and as a direct consequence, the connection between structure and mechanical properties has not been well established in many nc metals and alloys. Even the relatively simple-to-determine characteristics such as texture, grain size distribution, grain shape through the cross-section, and population of growth twins are often not well defined. However, in order to create maximum synergy between simulation and experiment, detailed information on the microstructure is necessary such as a distribution of the lattice misorientation and the GB plane misorientation, parameters that are accessible for coarse-grained material by means of sequential sectioning in a scanning electron microscope [143] or by analysis with a 3D-X-ray microscope [144]. Information of such type would facilitate a one-to-one copy of the sample in the computational model. Unfortunately, these techniques presently do not have the spatial resolution needed for nc metals.

Another common problem is the inability to reproduce microstructures even within a single processing route. Frequently, there is a wide distribution of grain sizes that varies from batch-to-batch and it is not obvious which segment of the distribution dominates the response to an applied stress. Furthermore, limitation in material availability has placed significant constraints on the number of mechanical tests performed in an investigation, raising additional questions on the reliability of the reported data.

This is an emerging field where findings from computations (primarily using large-scale molecular dynamics simulations) have far outpaced experimental observations. As a consequence, several fundamental theories and models remain to be validated with careful experiments. The computational models are only beginning to incorporation of realistic structural features including impurity and defect populations. A limitation of the computations is that molecular dynamics can only cover the very initial stages of the deformation. Thus, while structural information (e.g. grain boundary structure) and information pertaining to the very early stages of deformation (e.g. emission of a few dislocations from a boundary or motion of a few atoms at a boundary) may be considered reliable, evolution of damage and final fracture are all substantially affected by the starting microstructure and its consequence on microstructural evolution.

Comprehension of the deformation and fracture of nanocrystalline metallic materials at temperatures of the order of 0.1–0.2 of the melting temperature (e.g Cu, Ni, Co and Fe and their alloys) must accommodate i) the macroscopic observation of minimal tensile ductility in these materials, ii) the observation of intense localized deformation bands (shear bands), more prominent in the bcc metals and alloys (not reported thus far at quasi-static strain rates in nanocrystalline Ni or Cu), iii) the general acceptance of dislocation-mediated deformation at grain sizes of 30–40 nm and iv) the observation of dimpled rupture on the fracture surfaces, with the scale of dimples being significantly larger than the grain size but yet scaling with grain size.

A limited amount of systematic experimental information [98] has revealed that considerable opportunities exist for the design of highly damage-tolerant structural components through the judicious use of nc metals and alloys. For example, the results shown in Figs. 9 and 10 indicate that grain refinement with nc metals can impart improved resistance to fatigue crack nucleation under predominantly high cycle fatigue loading. However, such grain refinement strategies can lead to a detrimental effect on subcritical crack growth.

It is conceivable that layered and/or graded microstructures with nc grains at critical sites of crack nucleation, such as at free surfaces and in the immediate vicinity of stress concentrations, may lead to better overall damage tolerance in components made primarily of lower strength, higher ductility mc alloys.

Recent experimental work [145] has also shown that some nc metals offer improved resistance to damage evolution in monotonic and repeated sliding compared to ufc metals. Furthermore, it is also known that the addition of W to nc Ni can impart improvements in the tribological resistance [33]. Capitalizing on this potential for improving the scratch resistance and tribological properties of engineering structures by the proper design of surface layers with nc metals and alloys thus constitutes an interesting area that is rich in scientific and technological opportunities.

Acknowledgements

SS and KSK gratefully acknowledge support from the Defense University Research Initiative on NanoTechnology (DURINT) on "Damage- and Failure-Resistant Nanostructured and Interfacial Materials" which is funded at the Massachusetts Institute of Technology (MIT) by the Office of Naval Research under grant N00014-01-1-0808. The authors also acknowledge additional support from the Division of Materials Sciences and Engineering, Office of Basic Energy Sciences, U.S. Department of Energy under contract DE-AC05-00OR22725 with UT-Battelle, LLC. HVS acknowledges the support provided by several grants of the Swiss National Science Foundation and the CTI-program TOPNANO21. We thank Drs. M. F. Chisholm and J.A. Horton of Oak Ridge National Laboratory for their assistance with the transmission electron microscopy.

References

[1] Gleiter H. Acta Mater 2000;48:1.
[2] Hall EQ. Proc Soc London 1951;B64:747.
[3] Petch NJ. J Iron Steel Inst 1953;174:25.
[4] Ashby MF. Philos Mag 1982;A46:737.
[5] McFadden SX, Mishra RS, Valiev RZ, Zhilyaev AP, Mukherjee AK. Nature 1999;398:684.
[6] Lu L, Sui ML, Lu K. Science 2000;287:1463.
[7] McFadden SX, Sergueeva AV, Mishra RS, Mukherjee AK. Mater Sci Tech 2000:16;1340.
[8] Horita Z, Furukawa M, Nemoto M, Barnes AJ, Langdon TG. Acta Mater 2000;48:3633.
[9] Komura S, Horita Z, Furukawa M, Nemoto M, Langdon TG. Metall Mater Trans 2001;32A:707.
[10] Mishra RS, Valiev RZ, McFadden SX, Islamgaliev RK, Mukherjee AK, Philos Mag A 2001;81:37.
[11] Xu C, Furukawa M, Horita Z, Langdon TG. Adv Engin Mater 2003;5:359.
[12] Koch CC. Nanostruct Mater 1997;9:13.
[13] Zhang X, Wang H, Scattergood RO, Narayan J, Koch CC. Mat Sci Eng 2003;A 344:175.
[14] Tellkamp VL, Melmed A, Lavernia EJ. Metall Mater Trans 2001;32A:2335.
[15] Zhou F, Liao XZ, Zhu YT, Dallek S, Lavernia EJ, Acta Mater 2003;51:2777.
[16] Valiev RZ, Islamgaliev RK, Alexandrov IV. Prog Mater Sci 2000;45:103.
[17] Gleiter H, Prog Mater Sci 1989;33:223–315.
[18] Sanders PG, Fougere GE, Thompson LJ, Eastman JA, Weertman JR, Nanost Mater 1997;8:243.
[19] Sanders PG, Eastman JA, Weertman JR, Acta Mater 1997;45:4019.
[20] Erb U. Nanost Mater 1995; 6:533.
[21] El-Sharik AM, Erb U, Palumbo G, Aust KT. Scripta Metall Mater 1992;27:1185.
[22] Ebrahimi F, Zhai Q, Kong D. Scripta Mater 1998;39:315.
[23] He G, Eckert J, Loser W, Schultz L, Nature Mater 2003;2:33.
[24] He G, Zhang ZF, Loser W, Eckert J, Schultz L. Acta Mater 2003;51:2383.
[25] Inoue A, Zhang T, Masumoto T. Mater Trans Jpn 1990;31:177.
[26] Peker A, Johnson WL. Appl Phys Lett 1993;63:2342.
[27] Wang JG, Choi BW, Nieh TG, Liu CT. J Mater 2000;15:798.
[28] He Y, Poon SJ, Shiflet GJ. Science 1998;241:1640.
[29] Kim JJ, Choi Y, Suresh S, Argon AS. Science 2002;295:654.
[30] Markmann J, Bunzel P, Rosner H, Liu KW, Padmanabhan KA, Birringer R, Gleiter H, Weissmüller J. Scripta Mater 2003;49:637.
[31] Lu L, Li SX, Lu K. Scripta Mater 2001;45:1163.
[32] Schuh C, Nieh TG, Yamasaki T. Scripta Mater 2002;46:735.
[33] Schuh C, Nieh TG, Iwasaki H. Acta Mater 2003;51:431.
[34] Nanofoils from Integran Technologies Inc., Toronto, Canada (http://www.Integran.com).
[35] Dalla Torre F, Van Swygenhoven H, Victoria M. Acta Mater 2002;50:3957.
[36] Ebrahimi F, Bourne GR, Kelly MS, Matthews TE, Nanost Mater 1999;11:343.

[37] El-Sherik AM, Erb U. Jour Mater Sci 1995;30:5743.
[38] Schaefer HE, Würschum R, Birringer R, Gleiter H. Phys Rev B 1988;38:4595
[39] Van Petegem S, Dalla Torre F, Seegers D, Van Swygenhoven H, Scripta Mater 2003;48:17.
[40] Weertman JR. Mechanical behaviour of nanocrystalline metals in nanostructured materials: Processing, properties, and potential applications. Norwich: William Andrew Publishing, 2002.
[41] Kumar KS, Suresh S, Chisholm MF, Horton JA, Wang P. Acta Mater 2003;51:387.
[42] Zhu X, Birringer R, Herr U, Gleiter H. Phys Rev B 1987;35:9085.
[43] Herr U, Jing J, Birringer R, Gonser U, Gleiter H. Appl Phys Lett 1987;50:472.
[44] Haubold T, Birringer R, Lengeler B, Gleiter H. J Less-Comm Metals 1988;145:557.
[45] Wunderlich W, Ishida Y, Maurer R. Scripta Metall Mater 1990;24:403.
[46] Keblinski P, Wolf D, Phillpot SR, Gleiter H. Scripta Mater 1999;41:631.
[47] Siegel RW, Thomas GJ. Ultramicroscopy 1992;40:376.
[48] Thomas GJ, Siegel RW, Eastman JA. Scripta Metall Mater 1990;24:201.
[49] Van Swygenhoven H, Farkas D, Caro A. Phys Rev B 2000;62:831.
[50] Mills MJ, Daw MS. MRS Proceedings 1990;183:15.
[51] Hasnaoui A, Van Swygenhoven H, Derlet PM. Acta Mater 2002;50:3927.
[52] Weertman JR, Sanders PG. Solid State Phenom 1994;35–36:249.
[53] Keblinski P, Phillpot SR, Wolf D, Gleiter H. Acta Mater 1997;45:987.
[54] Hou M, Kharlamov VS, Zhurkin EE. Phys Rev B 2002;66:195408.
[55] Meyer R. MRS Symposium Proceedings 2000;634:B8.8.1.
[56] Keblinski P, Wolf D, Gleiter H. Interface Sci 1998;6:205.
[57] Voronoi GZ. Reine Angew Math 1908;134:199.
[58] Van Swygenhoven H. Science 2002;April 5:66.
[59] Schiøtz J, Di Tolla FD, Jacobsen KW. Nature 1998;391:561.
[60] Van Swygenhoven H, Spaczer M, Farkas D, Caro A. Nanostruct Mat 1999;12:323.
[61] Yamakov V, Wolf D, Phillpot SR, Mukherjee AK, Gleiter H. Nature Materials 2002;1:1.
[62] Yamakov V, Wolf D, Salazar M, Phillpot SR, Gleiter H. Acta Mater 2001;49:2713.
[63] Derlet PM, Hasnaoui A, Van Swygenhoven H. Scripta Mater 2003;49:629.
[64] Honeycutt DJ, Anderson HC. J Phys Chem 1987;91:4950.
[65] Derlet PM, Van Swygenhoven H. Phys Rev B 2002;67:14202.
[66] Cormier J, Rickman JM, Delph TJ. J Appl Phys 2001;89:99.
[67] Van Swygenhoven H, Derlet PM, Budrovic Z, Zeits fur Metall 2003 (in press).
[68] Van Petegem S. Positron annihilation study of nanocrystalline materials, Doctoral Thesis, University of Ghent, 2003.
[69] Legros M, Elliott BR, Rittner MN, Weertman JR, Hemkar KJ. Philos Mag A 2000;80:1017–1026.
[70] Wang YM, Wang K, Pan D, Lu K, Hemker KJ, Ma E. Scripta Mat 2003;48:1581.
[71] Jeong DH, Erb U, Aust KT, Palumbo G. Scripta Mater 2003;48:1067.
[72] Chokshi AH, Rosen A, Karch J, Gleiter H. Scripta Metall 1989;23:1679.
[73] Masumura RA, Hazzledine PM, Pande CS. Acta Mater 1998;46:4527.
[74] Ma E. Scripta Mater 2003;49:663.
[75] Jia D, Ramesh KT, Ma E. Acta Mater 2003;51:3495.
[76] Carsley JE, Fisher A, Milligan WW, Aifantis EC. Metall Mater Trans 1998;29A:2261.
[77] Sanders PG, Youngdahl CJ, Weertman JR. Mater Sci Eng A 1997;234–236:77.
[78] Vinogradov A, Hashimoto S. Advanced Engineering Materials 2003;5:351.
[79] Robertson IM, Birnbaum HK. Acta Metall 1986;34:353.
[80] Hull D, Bacon DJ. Introduction to dislocations. 4th ed. Butterworth-Heinemann, 2001.
[81] Weertman J, Weertman JR. Elementary dislocation theory. Oxford University Press, 1992.
[82] Whang S, Nishimura C, McCormick PG. Scripta Mater 2001;44:1507.
[83] Popov AA, Pyshmintsev I Yu, Demakov SL, Illarionov AG, Lowe TC, Sergeyeva AV, Valiev RZ. Scripta Mater 1997;37:1089.
[84] Karimpoor AA, Erb U, Aust KT, Palumbo G. Scripta Mater 2003;49:651.
[85] Zhang X, Wang H, Scattergood RO, Narayan J, Koch CC, Sergueeva AV, Mukherjee AK. Acta Mater 2002;50:4823.
[86] Wang N, Wang Z, Aust KT, Erb U. Mater Sci Eng 1997;A237:150.
[87] Mukai T, Suresh S, Kita K, Sasaki H, Kobayashi N, Higashi K, Inoue A. Acta Mater 2003;51:4197.
[88] Schwaiger R, Moser B, Dao M, Chollacoop N, Suresh S. Acta Mater 2003;51:5159.
[89] Mirshams RA, Xiao CH, Whang SH, Yin WM. Mater Sci and Eng 2001;A315:21.
[90] Hanlon T, Prchlik L, Suresh S. unpublished results (2003).
[91] Suresh S. Fatigue of materials. 2nd ed. Cambridge, UK: Cambridge University Press, 1998.
[92] Vasudevan AK, Sadananda K, Rajan K. Inter Jour of Fatigue 1997;19:S151–S159.
[93] Suresh S. Metall Trans 1985;16A:249.
[94] Agnew SR, Weertman JR. Mater Sci and Eng A 1998;A244:145.
[95] Agnew SR, Vinogradov A Yu, Hashimoto S, Weertman JR. Jour of Elec Mater 1999;28:1038.
[96] Mughrabi H, Höppel HW. Mater Res Symp Proc 2001;634:B2.1.1.
[97] Feltner CE, Laird C. Acta Metall 1967;15:1621.
[98] Hanlon T, Kwon Y-N, Suresh S. Scripta Mater 2003;49:675.

[99] Han BQ, Lee Z, Nutt SR, Lavernia EJ, Mohamed FA. Metall Mater Trans A 2003;34:603.
[100] Van Swygenhoven H, Spaczer M, Caro A. Acta Mater 1999;47:3117.
[101] Van Swygenhoven H, Derlet PM. Phys Rev B 2001;64:224105.
[102] Van Swygenhoven H, Derlet PM, Hasnaoui A. Phys Rev B 2002;66:24101.
[103] Derlet PM, Van Swygenhoven H, Hasnaoui A. Phil Mag A 2003 (in press).
[104] Derlet PM, Van Swygenhoven H. Scripta Mater 2002;47:719.
[105] Hasnaoui A, Van Swygenhoven H, Derlet PM. Phys Rev B 2002;66:184112.
[106] Hasnaoui A, Van Swygenhoven H, Derlet PM. Science 2003;300:1550
[107] Van Swygenhoven H, Spaczer M, Caro A, Farkas D. Phys Rev B 1999;60:22.
[108] Van Swygenhoven H, Caro A. Phys Rev B 1998;58:11246.
[109] Schiøtz JT, Vegge T, Di Tolla FD, Jacobsen KW. Phys Rev B 1999;60:11971.
[110] Yamakov V, Wolf D, Phillpot SR, Gleiter H. Acta Mater 2002;50:61.
[111] Sutton AP, Balluffi RW. Interfaces in crystalline materials. New York: Oxford Science, 1996.
[112] Yamakov V, Wolf D, Phillpot SR, Gleiter H. Acta Mater 2002;50:5005.
[113] Feichtinger D, Derlet PM, Van Swygenhoven H. Phys Rev B 2003;67:24113.
[114] Kelchner CL, Plimpton SJ, Hamilton JC, Phys Rev B 1998;58:85.
[115] Zimmerman JA, Kelchner CL, Klein PA, Hamilton JC, Foiles SM. Phys Rev Lett 2001;87:165507.
[116] Kiely JD, Houston JE. Phys Rev B 1998;57:12588.
[117] Ortiz M, Phillips R. Adv Appl Mech 1999;36:1.
[118] Gerberich WW, Nelson JC, Lilleodden ET, Anderson P, Wyrobek JT. Acta Mater 1996;44:3585.
[119] Li J, Van Vliet KJ, Zhu T, Yip S, Suresh S. Nature 2002;418:307.
[120] Van Vliet KJ, Li J, Zhu T, Yip S, Suresh S. Phys Rev B 2003;67:104105.
[121] Bragg WL, Nye JF. Proc Roy Soc London, Series A 1947;A190:474.
[122] Gouldstone A, Van Vliet KJ, Suresh S. Nature 2001;411:656.
[123] Van Vliet KJ, Tsikata S, Suresh S. Appl Phys Lett 2003;83(5):xxx.
[124] Murayama M, Howe JM, Hidaka H, Takaki S. Science 2002;295:2433.
[125] Ovid'ko IA. Science 2002;295:2386.
[126] Cai B, Kong QP, Cui P, Lu L, Lu K. Scripta Mater 2001;45:1407.
[127] Sanders PG, Rittmeer M, Kiedaisch E, Weertman J, Kung H, Lu YC. Nanost Mater 1997;9:433.
[128] McFadden SX, Sergueeva AV, Kruml T, Martin J-L, Mukherjee AK. MRS Proceedings 2001;634:B1.3.1.
[129] Youngdahl CJ, Weertman JR, Hugo RC, Kung HH. Scripta Mater 2001;44:1475.
[130] Milligan WW, Hackney SA, Ke M, Aifantis EC. Nanostr Mater 1993;2:267.
[131] Hugo RC, Kung H, Weertman JR, Mitra R, Knapp JA, Follstaedt DM. Acta Mater 2003;51:1937.
[132] Derlet PM, Van Swygenhoven H. Philos Mag A 2002;82:1.
[133] Farkas D, Van Petegem S, Van Swygenhoven H. unpublished results, 2003
[134] Müllner P, Solenthaler C, Speidel MO. Acta Metall Mater 1994;42:1727.
[135] Embury JD, Szczerba MS, Basinski ZS. In: Yoo MH, Wutig M, editors. Twinning in advanced materials, Warrendale, PA: The Minerals, Metals and Materials Society; 1994, p. 331–336.
[136] Gray III GT. Acta Metall 1988;36:1745.
[137] Chen M, Ma E, Hemkar KJ, Sheng H, Wang Y, Cheng X. Science 2003;300:1275.
[138] Thomson CB, Randle V. Scripta Mater 1996;35:385.
[139] Aust KT, Erb U, Palumbo G. Mater Sci Eng 1994;A176:329.
[140] Müllner P, Solenthaler C, Speidel MO. In: Yoo MH, Wutig M, editors. Twinning in advanced materials, Warrendale, PA: The Minerals, Metals and Materials Society; 1994, p. 483–490.
[141] Farkas D, Van Swygenhoven H, Derlet PM. Physical Review B 2002;66:60101.
[142] Nakahara S. Acta Metall 1988;36:1669.
[143] Sylor DM, Rohrer GS. J Am Ceram Soc 2002;85:2799.
[144] Poulson HF, Nielsen SF, Lauridsen EM, Schmidt S, Suter RM, Lienert U, Margulies L, Lorentzen T, Juul Jensen D. J Appl Cryst 2001;34:751.
[145] Hanlon T, Suresh S. unpublished results, MIT; 2003.